SYNCHRONIZATION IN BIOLOGICAL SYSTEMS

By

Jonathan P. Klaas

RECOMMENDED:

Advisory Committee Chair

Chair, Department of Physics

APPROVED:

Dean, College of Natural Science and Mathematics

Dean of the Graduate School

December 7, 2004

Date

SYNCHRONIZATION IN BIOLOGICAL SYSTEMS

A

THESIS

Presented to the Faculty

of the University of Alaska Fairbanks

in Partial Fulfillment of the Requirements

for the Degree of

MASTER OF SCIENCE

By

Jonathan P. Klaas, B.S.

Fairbanks, Alaska

December 2004

Abstract

Synchronization, the adjustment of rhythms via coupling, is an essentially nonlinear effect in coupled dynamical systems. Synchronization is observed in many systems, for example the moon's periods of rotation and revolution, in pendulums suspended from a common support, in swarms of fireflies that flash in unison, and in biological circadian rhythms. Circadian rhythms are periodic fluctuations in multiple physiological systems that have evolved as a consequence of the daily rotation of the earth. These rhythms have been observed in organisms ranging from cyanobacteria to man. In this thesis we will present a conceptually simple model of circadian rhythms to yield insight into the activity patterns of mice in light and food restriction experiments. The model consists of two coupled van der Pol oscillators that are driven by an external periodic influence representing food availability. The results of the model are compared to circadian data of mice collected by Dr. Abel Bult-Ito (Institute of Artic Biology).

Table of Contents

List of Figures

Acknowledgements

Dr. Renate Wackerbauer, for guidance, support, and many discussions.

Dr. David Newman and the complex systems group, for keeping physics interesting.

Dr. Abel Bult-Ito, Kelly Hochstetler, Maria Castillo, and Ron for providing the raw data and a view from the biological perspective.

Last, but not least, my wife, for love and encouragement.

Chapter 1

Introduction

Circadian rhythms are periodic fluctuations in various physiological systems that seem to be a response to the daily rotation of the earth and subsequent effects. However, circadian rhythms are not merely a physiological 'echo' of the external period, as they can provide a mechanism to predict future periodic events such as sunrise or food availability, and can also persist in the absence of any external time cue such as a periodic light-dark cycle [2]. These rhythms have been observed in plants, animals, fungi, protozoa, and cyanobacteria [3]. The mechanism by which the external period influences these physiological systems is primarily (but not only) exposure to sunlight. For humans, circadian rhythms may play a role in heart attacks and stroke, as both are more likely to occur in mid-morning [4], possibly reflecting complex interactions between the circadian system and other physiological functions. Chronopharmacology [5] is a new area of medicine that takes circadian rhythms into account, with the goal of better understanding the interactions between medication and the circadian cycle. Study of circadian systems may also prove beneficial to people who work night shifts, submariners, and those who travel often by air across multiple time zones, inducing jet-lag [3].

Synchronization, the adjustment of rhythms via coupling, is an essentially nonlinear effect in coupled periodic systems. Synchronization is observed in many systems, for example the moon's periods of rotation and revolution, in pendulums suspended from a common support, and in swarms of fireflies that flash in unison [6]. Modern society utilizes synchronization in electrical power grids, communication systems, and lasers. Human life depends

on the synchronization of cells in the heart and brain [6].

In this thesis we present a simple model of the mammalian circadian system that mimics activity patterns of mice under food and light restriction experiments (data from Dr. Abel Bult-Ito, Institute of Arctic Biology, Fairbanks, Alaska [1, 7]). The goal of this model is to provide intuition and insight into this particular circadian system and into biological circadian systems in general. This model is based on nonlinear dynamical phenomena wherein oscillators with similar frequencies ω_1 and ω_2 adjust their individual frequencies to a common frequency $\bar{\omega}$ when coupled together. We analyze how this system interacts with a drive that represents the availability of food. In the biological experiment, food acts as a time cue that can synchronize the circadian system. We then compare our model to experimental data taken from mice [1, 7], and draw conclusions about the interactions of different biological systems required to produce the observed data.

In the first chapter we introduce the dynamics of basic nonlinear oscillatory systems. We focus on the dynamics that will be specific to our model, and provide methods to quantify these dynamics. The concept of synchronization will be defined and explained, which will provide a convenient abstraction when dealing with coupled oscillators. In the second chapter we motivate our model of circadian systems. We provide an overview of other studies of circadian rhythms, and present data to argue for the validity of our simple model. The third chapter is a comparison between experimental mouse activity data and data generated by our model. We analyze wheel running data from mice [1, 7] exhibiting three distinct classes of behavior, and show how each is recreated using our model. We also analyze the parameter space composed of the coupling coefficients and use this to show that certain potential model simplifications do not fit the experimental data. The final chapter is a discussion of the concepts we have covered, and of the relationship of our model to experimental knowledge of circadian systems.

Chapter 2

Nonlinear Dynamics

2.1 Dynamical Systems

A system that can be described by a differential or difference equation can be identified at any moment of time as existing in some state. A state is described by a set of classifiers that uniquely identify our system in time; e.g., the state of a free particle is often described by its position and velocity. Dynamics is the study of how systems change states, and the particular sequence of states that a dynamical system moves through is referred to as its trajectory. In this thesis we will be limited to deterministic systems, which means that given an initial state and the equations describing the system we can calculate the trajectory for an arbitrary amount of time.

2.1.1 The van der Pol oscillator

Proposed by B. van der Pol in the 1920s as an equation describing the behavior of an electrical triode [8], the van der Pol (VDP) equation is one of the most analyzed [9–11] nonlinear systems. Furthermore, it will play a major role in our coupled oscillator model and it makes a useful example for discussing dynamics. The VDP equation represents the harmonic oscillator equation with a position dependent damping term,

$$\ddot{x} = \epsilon(1 - x^2)\dot{x} - \omega_0^2 x. \tag{2.1}$$

For small amplitudes ($|x| < 1$) the nonlinear term acts as an energy source, and for large amplitudes ($|x| > 1$) it provides damping. The coefficient ϵ has been referred to as the stiffness parameter [12]. For values of $\epsilon \ll 1$ the system is quasi-linear and the observed frequency of the system is close to ω_0, the 'natural frequency', but not identical to it due to the effect of the nonlinear term. When $\epsilon \gg 1$ the system becomes what is known as a stiff, or relaxation oscillator because the period of oscillation $\tau \approx \epsilon$ which is characteristic of the time of discharge (relax) of a capacitor [8].

2.1.2 Phase space

A system described by a second-order differential equation such as Eqn. (2.1) can be rewritten as two first-order equations.

$$\dot{x} = y \tag{2.2a}$$

$$\dot{y} = \epsilon(1 - x^2)y - \omega_0^2 x \tag{2.2b}$$

Two dynamical variables (x, y) are needed to describe the state. This means that knowledge of the generalized position x and the velocity y provides full information about the system. Plotting y versus x from Eqn. (2.2) results in a 'phase space' or 'state space' diagram in which a point completely specifies the state of the system [10]. Depicted in Figs. 2.1[a-c] are three van der Pol oscillators with differing parameters, each oscillator beginning its trajectory at two different initial conditions. By converting to a polar coordinate system, the instantaneous state of the oscillator is a point on the trajectory and can be referenced with an angle θ and an amplitude r. Often in phase space diagrams such as this, θ is measured in a clockwise fashion with respect to the positive x axis, as this is the direction of rotation of the harmonic oscillator as time increases. Figure 2.1[a] shows the van der Pol oscillator in the limit ($\epsilon \to 0$), the harmonic oscillator. The trajectory rotates in an ellipse about the origin with r dependent only on the initial conditions. Cases [b,c] of Fig. 2.1 show so called 'quasi-linear' and 'stiff' van der Pol oscillators, respectively. In both cases the trajectories spiral toward a closed orbit that is independent of the initial conditions. This type of trajectory is known as a 'limit cycle'.

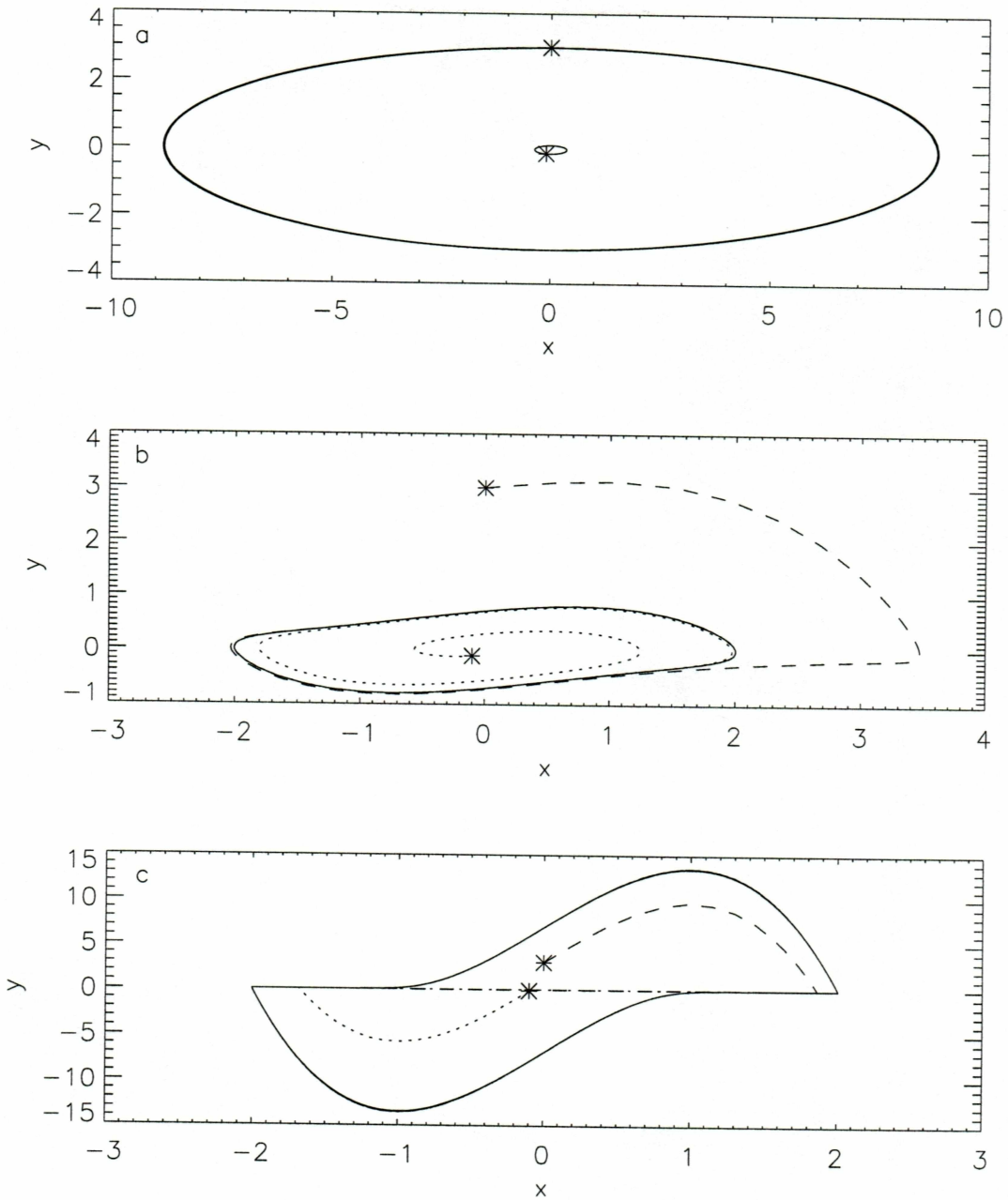

Figure 2.1. Phase space diagrams of the VDP oscillator (Eqn. (2.1)) with differing initial conditions: a) $\epsilon = 0$, the VDP oscillator reduces to the simple harmonic oscillator, with each initial condition on a closed orbit; b) $\epsilon = 0.23$, the quasi-linear oscillator displays limit cycle behavior; c) $\epsilon = 10$, the stiff oscillator displays limit cycle behavior. Initial conditions are identical between plots and are marked with an asterisk. The natural frequency $\omega_0^2 = 0.115$ for all plots.

2.1.3 Limit cycles

According to the Poincaré-Bendixson Theorem [9], for a two-dimensional phase space that contains no trajectories that go to infinity, only three possibilities exist for trajectories as time $t \to \infty$:

1. Fixed points;

2a. Closed orbits;

2b. Limit cycles.

This is not surprising after considering the Uniqueness Theorem [13, p.347] for ordinary differential equations, which guarantees a unique trajectory for each initial condition. This means that any trajectory described by an ordinary differential equation can never cross itself because the point of intersection could be selected as an initial condition and would lie on two different trajectories, thereby violating the Uniqueness Theorem. If trajectories that head to infinity are ignored, only periodic solutions remain, where a fixed point has a period of zero. The closed orbit of the harmonic oscillator is not referred to as a limit cycle, as every state lies on a periodic solution. In contrast, limit cycles are characterized by Fig. 2.1[b,c], where trajectories near the periodic solution are attracted, or in other cases repelled from it.

2.1.4 Phase

In this study, phase is the primary identifier of an oscillator's state. The archetypal example is the sinusoidal function $y = sin(\phi)$, where ϕ is the phase. Often phase is limited to the interval $[0, 2\pi]$, as this conveys complete information about simple isolated oscillators since one period is identical to the next. For coupled oscillators however, it is often useful to not restrict the phase interval, but to allow the phase difference between two oscillators to exceed 2π. Each additional factor of 2π in the phase difference amounts to an additional rotation by one of the oscillators in reference to another. The phase information of an oscillator is conserved when mapping an oscillator's trajectory to the unit circle. A state on the unit circle is quantified by its angular location and the number of previous rotations.

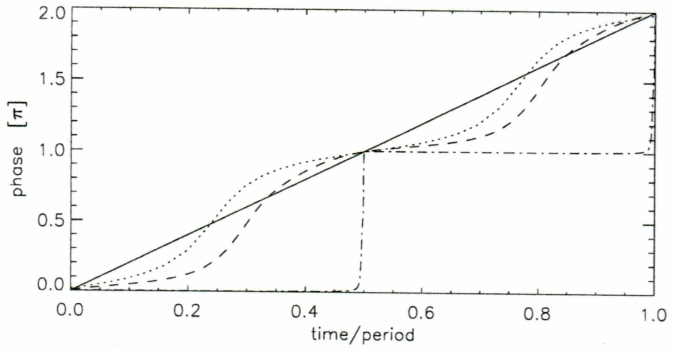

Figure 2.2. The phase of the VDP oscillator during one oscillation, as determined by two different measures (see text). The solid line corresponds to the uniform phase measure, while the partial lines show the polar angle for each of the three oscillators shown in Fig. 2.1: the harmonic oscillator (dotted line); the quasi-linear oscillator (dashed line); and the stiff oscillator (dot-dashed line). The periods of the three oscillators are scaled to 1.

2.1.5 Definitions of phase

In the case of a single limit cycle oscillator, once a trajectory approaches a limit cycle, complete information of the system can be specified by the polar angle in phase space because the amplitude can then be expressed as a function of this angle. This polar angle is one measure of the phase of the oscillator. But because trajectories can move with different velocities through different regimes in phase space, the time rate of change of the polar angle may not be constant. A simpler measure for the phase of a trajectory is to have the phase increase uniformly in time by 2π over each period, and we will refer to it as the 'uniform' phase measure. Figure 2.2 shows the uniform phase measure (solid line) and the polar angle for the three oscillators from Fig. 2.1. By construction, the uniform phase will always align with the polar angle at the beginning and end of each oscillation period, but elsewhere there is no guarantee of equality. In this example, the two measures also conform on multiples of π due to the symmetrical nature of the oscillations. In our model, we will mainly be concerned with the behavior of phase over many periods, so the uniform phase measure will provide sufficient information for our purposes.

For oscillating systems requiring more than two dimensions for a complete description, phase alone generally cannot identify a unique state. The possibilities for asymptotic states

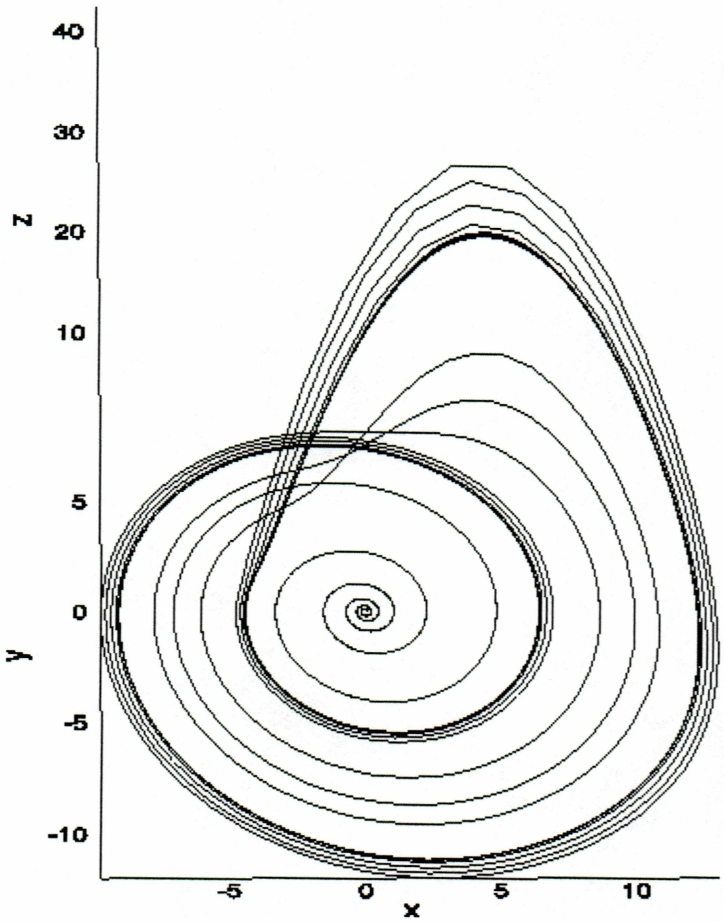

Figure 2.3. Rössler system in three dimensional phase space for the chaotic parameter range $a = b = 0.2$, $c = 5.7$. Trajectories appear to cross because of the projection into two dimensions. The Rössler system is described by the equations $\dot{x} = -z - y$, $\dot{y} = x + ay$, $\dot{z} = b + z(x - c)$

is no longer limited to closed orbit, limit cycle and fixed point behavior according to the Poincaré-Bendixson Theorem. A third dimension allows oscillatory trajectories to change amplitude without intersecting themselves. Examples of this behavior include the chaotic Lorenz and Rössler systems, the latter shown in Fig. 2.3. Much recent research has focused on defining phase for chaotic or experimentally observed systems by using the Hilbert transform [14–17] or the wavelet transform [15], though the polar angle measure remains useful [18–20].

2.2 Synchronization

The adjustment of rhythms via coupling (synchronization) was first observed by Huygens in the 17th century [5]; he noticed that pendulum clocks suspended from the same beam would slowly adjust their relative phases until the pendulums motion was anti-symmetric (having a phase difference of 180 degrees). Since then, synchronization has been observed in many systems including the human cardiorespiratory system [17, 21], the rat cardiorespiratory system [22], laser arrays [16], electrical circuits [23], and mammalian circadian rhythms [5]. In the literature, the phenomenon of synchronization has been referred to as entrainment [24], phase locking [5], phase trapping [25], frequency locking [5], frequency pulling [26], etc. While it is often the case that these different names refer to different types or degrees of synchronization, there is no universally recognized naming convention. Mainly this is due to the observation of synchronization across many different fields and the lack of communication between individual fields.

2.2.1 Definitions of Synchronization

The definitions of synchronization are as multiple as the names. Considering two oscillators with phases ϕ_1 and ϕ_2, we will define synchronization by

$$n\phi_1 - m\phi_2 = constant \tag{2.3}$$

where n, m is a pair of integers. This type of synchronization we will refer to as 'phase locking' where (n:m) designates the ratio of oscillation periods. An example of 1:1 synchronization (Fig. 2.4) could be two sinusoids with identical frequency but with different phase. Similarly, an example for synchronization of type 1:2 could be two sinusoids with the first sinusoid having frequency ω and the second having frequency $\omega/2$, thus allowing the first sinusoid to make exactly two oscillations for each oscillation of the second (Fig. 2.5).

A weaker condition for synchronization is given by

$$|n\phi_1 - m\phi_2| \leq constant. \tag{2.4}$$

This definition allows systems with bounded variations in phase to be defined as synchronized. We will refer to this case as 'frequency locking' as the relative phases may vary

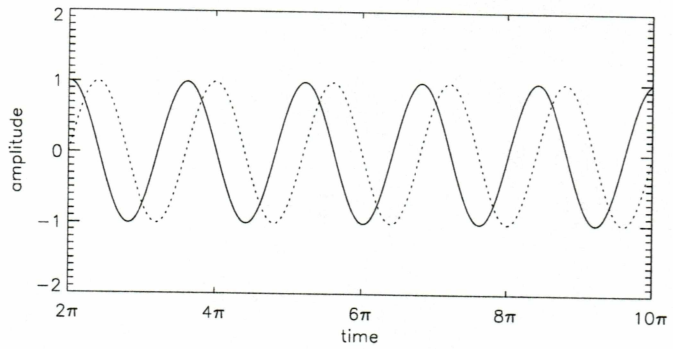

Figure 2.4. 1:1 phase locking in sinusoids with a small constant phase difference. The frequency is $\omega_0 = 0.2$

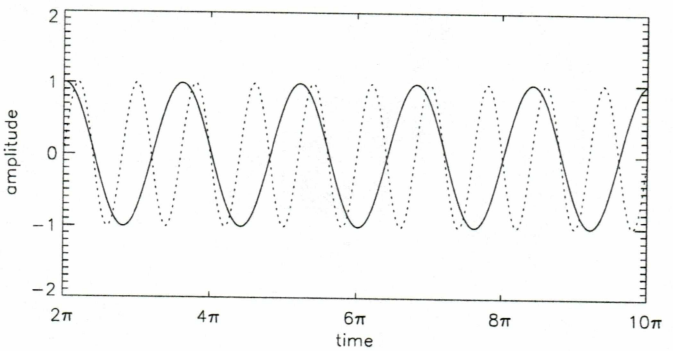

Figure 2.5. 1:2 phase locking in sinusoids with a small constant phase difference. The frequencies are $\omega_0 = 0.2$ (solid line) and $\omega_0 = 0.4$ (dashed line).

but the average frequency does not. For linear systems Eqn. (2.4) reduces to Eqn. (2.3) as bounded variations simply do not occur. For some nonlinear systems this distinction becomes evident. An even more general definition of synchronization [15, 16] relies on the statistical behavior of the phase relationship between two coupled oscillators, where a peak in the probability distribution of phase differences designates synchronization.

2.2.2 Arnold tongues

Linear systems such as the simple harmonic oscillators in Figs. 2.4 and 2.5 can be synchronized only when the frequencies of the component oscillators are identical. An analysis of

the driven, damped harmonic oscillator, as is found in undergraduate mechanics textbooks [27], shows that the primary effect of driving is an amplitude peak at the resonance frequency while the oscillators frequency is functionally independent of the driver frequency. For a nonlinear system however, synchronization occurs not only when the driver frequency ω_d is equal to the oscillators 'natural' frequency ω_0, but also when they are sufficiently close. For example, consider the driven VDP oscillator

$$\ddot{x} + \epsilon(1 - x^2)\dot{x} + \omega_0^2 x = k_d \sin \omega_d t \tag{2.5}$$

where ω_0 is the natural frequency, ω_d is the drive frequency, k_d is the driver coupling, and ϵ is the stiffness parameter. The frequency difference $\omega_d - \omega_0$ is referred to as the 'detuning' $\Delta\omega$. As the coupling strength k_d between the driver and the oscillator increases, larger detuning will result in synchronization. This means that for a small difference in frequencies, only a small coupling coefficient is required to entrain the oscillator to the drivers frequency, while larger frequency differences require larger coupling coefficients in order for synchronization to result.

Figure 2.6 shows the coupling strength-detuning parameter space for the driven VDP oscillator (Eqn. (2.5)) broken into regions of synchronization (black) and non-synchronization according to Eqn. (2.4) with $m = n = 1$. Named after the discoverer and for the distinctive shape, the synchronization regime is known as an Arnold tongue [5]. Within the Arnold tongue, the sinusoidal driver is adjusting the frequency of the oscillator to its own for the synchronization condition to be satisfied. Implicit to this observation is that ω_0 is not simply related to the observed period of the driven van der Pol oscillator. The tongue is not centered at zero detuning due to the nonlinear nature of the van der Pol oscillator. Theoretically, tongues of all integer ratios exist [5], and observations of some higher order locking in experimental systems have been made [23].

Figure 2.7 shows time series from three different regions relative to the Arnold tongue. In each plot the larger amplitude signal represents the x component of the VDP oscillator, (Eqn. (2.5)) and the smaller amplitude signal represents the sinusoidal drive (Eqn. (2.5)). The upper plot is for parameters on the Arnold tongue, and shows (1:1) synchronization between the driver and the oscillator. The middle plot depicts free running behavior which occurs far from an Arnold tongue. The lower plot depicts the transition region, near an

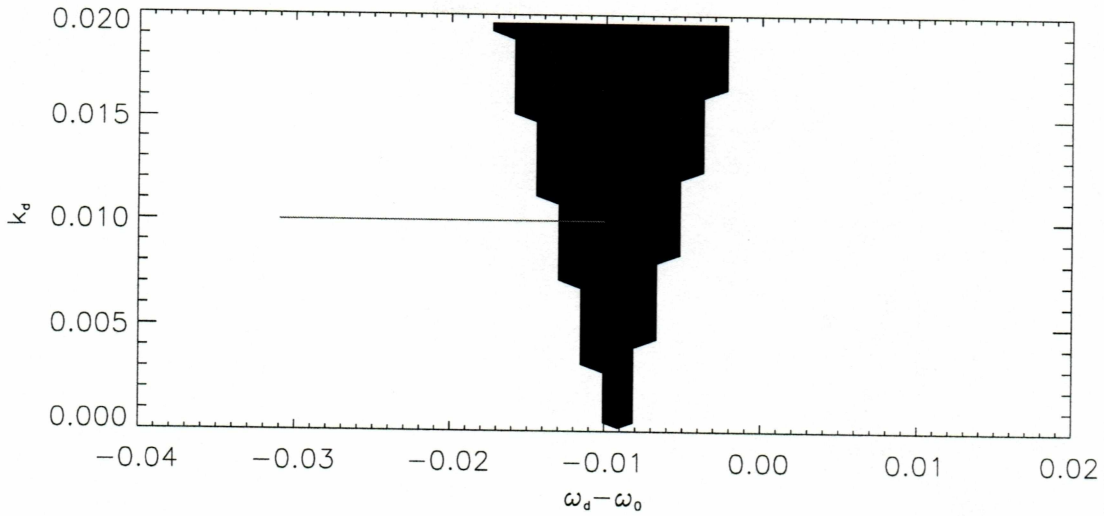

Figure 2.6. Synchronization of a van der Pol oscillator (Eqn. (2.5)) with a sinusoidal driver plotted in driver coupling (k_d) versus detuning ($\omega_d - \omega_0$) parameter space shows the Arnold tongue structure. The region of 1:1 frequency locking is plotted in black. Gray line indicates transition to synchronization. Rough edges are the result of the parameter resolution.

Arnold tongue but not in the region of parameter space representing synchronization.

2.2.3 The edge of synchronization: phase slips

Outside the region of synchronization the system experiences a gradual decrease in the degree of synchronization. This transition from synchronization is characterized by horizontal plateaus in the phase difference between driver and oscillator, where the oscillator and driver are slowly drifting apart, interspersed with brief intervals where the phase difference changes rapidly by 2π (Fig. 2.8). These sudden and rapid adjustments in relative phase are referred to as phase slips [5]. The abundance of phase slips when moving onto an Arnold tongue ranges from continuous phase adjustment to phase slips once in thousands of periods of oscillation (Fig. 2.8). The continuous phase adjustment is referred to as 'free running' because the oscillation frequency is closer to ω_0, the frequency where the system would oscillate if free of driving. Figure 2.8 shows the phase difference between the VDP oscillator and its sinusoidal driver sampled along the horizontal gray line in Fig. 2.6 at

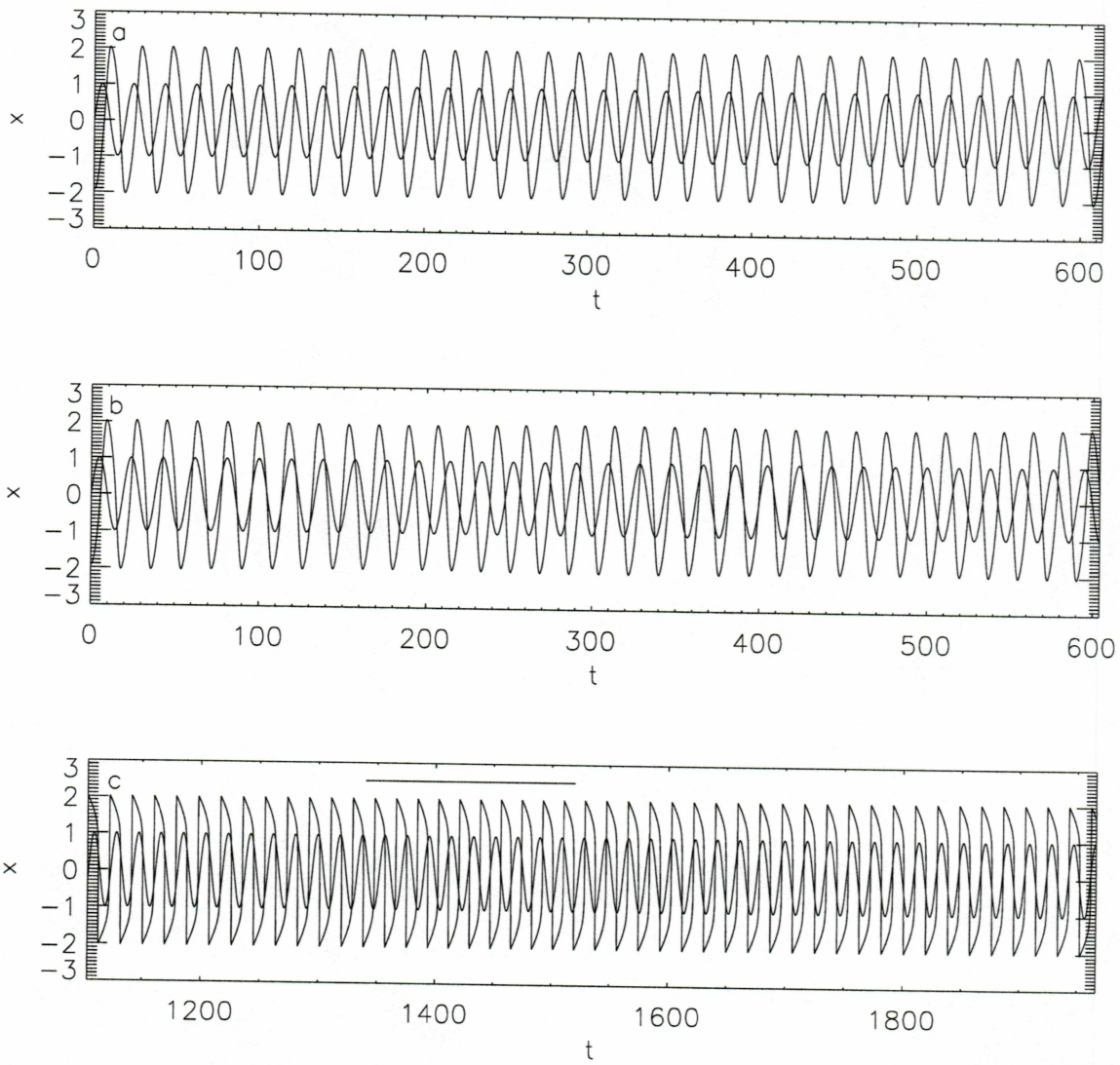

Figure 2.7. Time series of the x component of the driven VDP oscillator (large amplitude) and the drive (small amplitude), from Eqn. (2.5) for different degrees of locking. a) Near the center of the tongue: $\Delta\omega = -0.01$, $k_d = 0.01$, $\epsilon = 0.23$. b) 'Free running' behavior far from the range of entrainment $\Delta\omega = -0.016$, $k_d = 0.01$, $\epsilon = 0.23$. c) A single phase slip which occurs near the edge of an Arnold tongue $\Delta\omega = -0.69$, $k_d = 0.16$, $\epsilon = 10$, with the region of 'fast' phase change wherein the phase shifts by π indicated by a horizontal bar. The next 'fast' phase change begins at $t = 2750$. $\Delta\omega = \omega_d - \omega_0$, $\omega_d = 0.33$ for all cases.

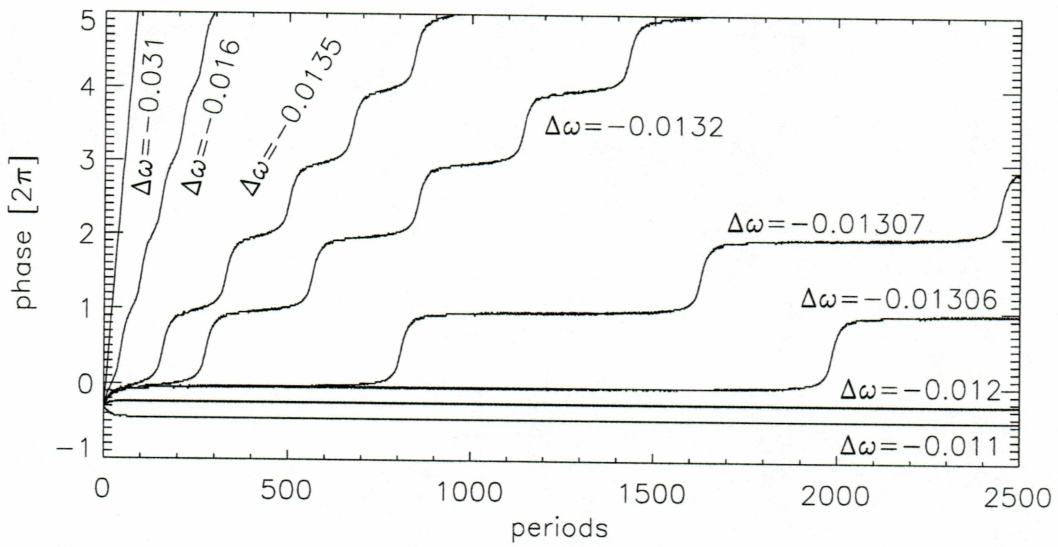

Figure 2.8. Phase difference between the VDP oscillator and its sinusoidal driver versus time. The natural frequency ω_0 of the VDP oscillator is varied following the horizontal line in Fig. 2.6 with the resultant detuning $\Delta\omega$ labeled on the graph, while the driver coupling k_d is kept constant at $k_d = 0.010$ and the drive frequency $\omega_d = 0.33$. The time is plotted in units of VDP oscillator periods.

driver coupling $k_d = 0.010$. The phase difference is defined as $\phi_{vdp} - \phi_{driver}$, so an oscillator with a larger period than its driver will produce a negative phase difference, as the driver's phase will increase faster in time. For each value k_d of the Arnold tongue there exists two critical drive frequencies ω_{c+} and ω_{c-} that define the edges of the tongue, between which no phase slips will occur. In this frequency locked domain the asymptotic phase relation is determined by the natural frequency of the VDP oscillator ω_0, as frequencies closer to the larger critical frequency will result in a more positive asymptotic phase relation, and vice versa. This is seen in Fig. 2.8 with detuning $\Delta\omega = -0.012$ and $\Delta\omega = -0.011$. As ω_0 nears the smaller critical frequency ω_{c-}, the asymptotic phase relation between driver and oscillator becomes gradually more negative, until ω_0 is smaller than ω_{c-} and phase slips occur in the negative sense.

Outside of the interval $[\omega_{c-}, \omega_{c+}]$, the length of the plateaus in Fig. 2.8 scales with the detuning $(\omega_c - \omega_0)$ according to

$$\tau \sim |\omega_c - \omega_0|^{-1/2} \tag{2.6}$$

where τ is the number of oscillator periods between successive phase slips, and ω_c is the closer of the two critical frequencies (Fig. 2.9). By making fine adjustments of the natural frequency ω_0 the time between phase slips can be increased until the detuning is limited by the numerical precision. When the detuning is small, τ becomes very large and diverges. The scaling relation fails for large detuning.

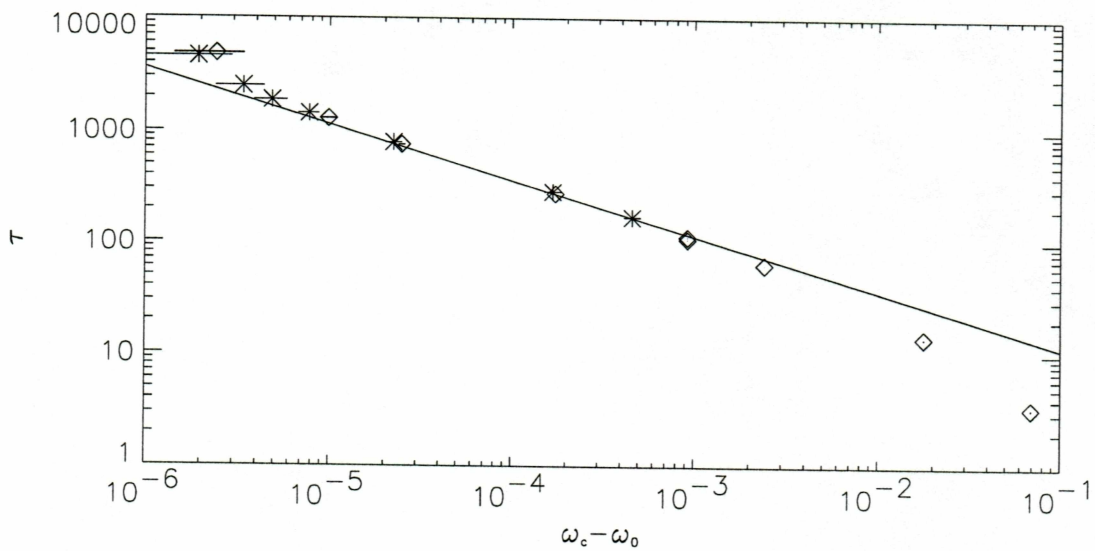

Figure 2.9. Scaling behavior of number of periods between successive phase slips versus $|\omega_c - \omega_0|$ (see text). Data points are shown for two different tongue boundaries. The solid line represents the scaling relation given in Eqn. (2.6) with a proportionality constant of 170.

Chapter 3

Of Mice and Men

Circadian rhythms, from the Latin 'circa diem' translated 'roughly a day' [3], correspond to a wide range of biological processes that occur with a 24 hour period in organisms ranging from cyanobacteria to humans. Examples of studied circadian processes are body temperature [12, 28], sleep-wake cycles [12, 29], and melatonin (a neurotransmitter) release [30], to name a few. In mammals these circadian rhythms are primarily controlled by the suprachiasmatic nuclei (SCN) [29, 31], an assemblage of neurons located just above the optic chiasm in the hypothalamus which receives input from the retina and other brain areas [32]. Circadian rhythms have been both extensively studied [3, 31, 33–40], and modeled [12, 26, 41–49]. In the 1990's, advances in genetics brought much new information to light about the biochemical source of these daily oscillations [3]. Yet much about these systems remains unknown, such as the structures responsible for the sleep-wake rhythm, the interaction between different circadian processes or the mechanisms of interaction with the environment. In light of this body of knowledge, we synthesize a minimalistic model that is capable of reproducing a wide range of observed behaviors in mice and we use this simplistic model to provide intuition into the dynamics of the circadian system.

3.1 Observations of circadian rhythms

Studies of circadian rhythms usually involve the recording of body temperature [29, 37, 39, 40], activity intervals [7, 31, 34, 37, 39, 40], cortisol [39, 40], and/or feeding or drinking

activity [29, 31, 37] from numerous individuals. Circadian systems have been observed being synchronized to light-dark cycles [40], food availability [7, 31] and animal cage changes [31]. In the absence of a time signal (zeitgeber) circadian systems are characterized by 'free-running' behavior [25], in which the system expresses its intrinsic period of approximately 24 hours, often with surprising precision. Evidence of this self-sustained oscillation is commonly observed in jet-lag, where after moving through multiple timezones it may take several days for the internal rhythm to adjust to the time-shifted environment. Czeisler et. al [40] found that a group of humans in an environment devoid of time cues for 3-4 weeks exhibited an average body temperature period of 24 h 11 m, with a standard deviation of 8 minutes. Other studies have found individual humans with free-running activity periods as large as 65 h and as short as 13 h [32].

3.2 Determining a Model for the Circadian System

3.2.1 Evidence for two oscillators

In 1969, Pavlidis noted, "It is generally accepted by most workers in this field that there exists a basic oscillating system in each organism which in turn drives a secondary system directly responsible for the observed, overt behavior [43]." Support for this statement is found in observations of human activity (or wake times) and temperature oscillations, where under normal conditions wake times and the temperature oscillation are synchronized (1:1 locking, Eqn. (2.4)) to the external light zeitgeber [25]. However in the absence of external time cues animals exhibit free-running behavior, which is the expression of an 'internal' or 'compromise' frequency of the system. Also commonly observed is 'internal desynchronization' [12, 25] wherein the temperature and activity rhythms which were synchronized during free run behavior begin to express distinct periods, often characterized by long intervals of slowly changing phase difference punctuated by short, rapidly changing intervals, highly reminiscent of phase slipping (Fig. 3.1). These three behaviors (synchronization, free running, phase slipping), are also observed in driven nonlinear oscillator systems, where the synchronized behavior occurs on an Arnold tongue, the phase slipping occurs near the boundary of an Arnold tongue, and the free running occurs farther away in parameter space.

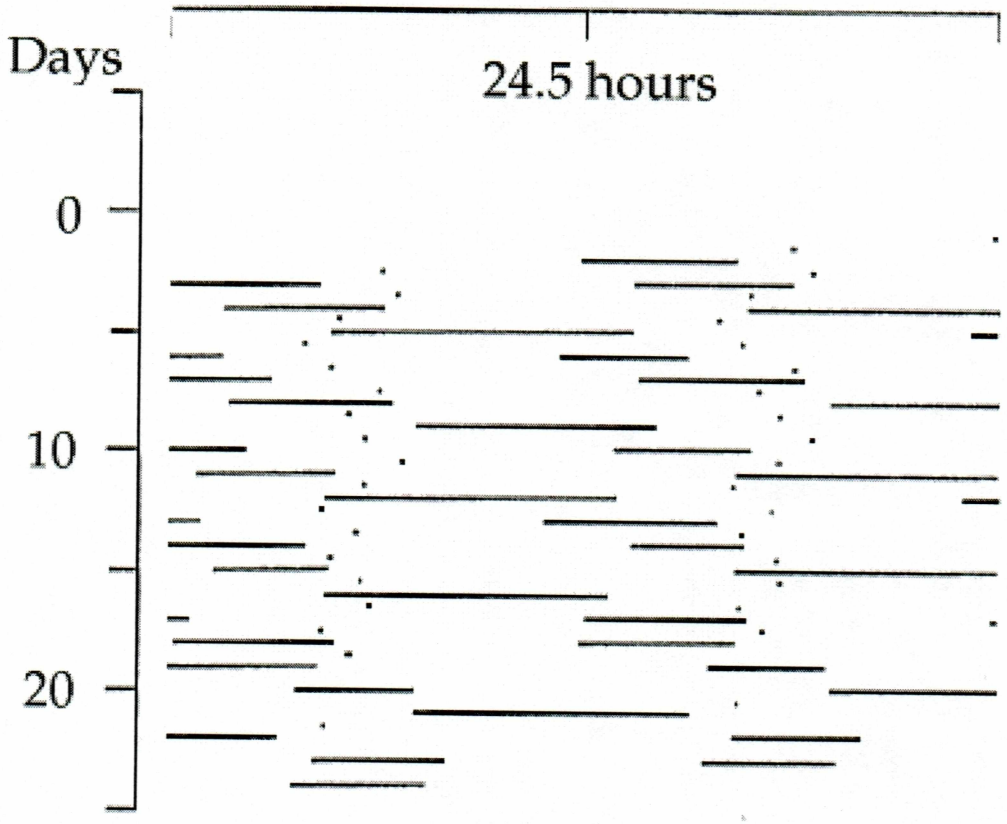

Figure 3.1. Human sleep-wake record with black bars indicating sleep, and dots indicating the time of temperature minimums. Two successive 24.5 hour 'circadian days' (determined by temperature data) are shown horizontally and advanced by one 24.5 hour interval for each line vertically to provide visual continuity (i.e. data are plotted twice). There seems to be a preferred phase relationship between the sleep-wake and temperature rhythms, but the sleep-wake cycle is unable to synchronize to the temperature cycle, and phase slipping occurs. The sleep-wake rhythm is desynchronized from the temperature rhythm. Reprinted from Strogatz p.44, figure 3-19 [25].

3.2.2 Evidence for limit cycle type oscillators

At the cellular level it has been shown that individual cells in the hamster suprachiasmatic nuclei exhibit different periods, and that the period of wheel running activity is determined by the mean period of the individual cells [50]. For weak coupling among cells, this system can be described by an approximate set of equations

$$\dot{\Theta}_i = \omega_i + \sum_j K_{ij} f(\Theta_j - \Theta_i) \tag{3.1}$$

for $i = 1, ..., N$ [50, 51]. Θ_i is the phase of the i^{th} cell, ω_i is its frequency in isolation, K_{ij} is a matrix of coupling coefficients, and $f(\Theta_j - \Theta_i)$ is some function that acts on neighboring cell phase differences. For certain conditions of K_{ij} and $f(\Theta)$, a population described by Eqn. (3.1) will synchronize to the mean frequency of the population, with the number of synchronized cells increasing as the average coupling strength is increased [52]. Replacing the system of oscillators (Eqn. (3.1)) with a single oscillator whose frequency is identical to the mean frequency of the population is an obvious simplification but nevertheless captures the stable synchronized dynamics [42, 51]. By this averaging, an ensemble of oscillatory cells can be modeled approximately as a single macroscopic oscillator.

Winfree showed that a phase-only oscillator (an oscillator described by a single dynamical variable) exhibits different behavior from a phase-amplitude oscillator (an oscillator described by two dynamical variables) when they are strongly perturbed [3]. These behavioral differences can be measured by careful experimentation, and they are used to determine whether the circadian system can be described by a phase-only oscillator. Many studies have been done to determine the effect of perturbations to the circadian system due to bright lights and light pulses [3, 35, 39] by comparing the phase of the oscillator before a perturbation to the phase following the perturbation. Doing this for all initial phases results in a phase response curve (PRC) as shown in Fig. 3.2 [3]. For weak perturbations, both phase-only and phase-amplitude oscillators will exhibit what is known as weak (type 1) resetting of their phase. For a sufficiently strong perturbation a phase-amplitude oscillator will exhibit strong (type 0) resetting, but a phase-only oscillator cannot show strong resetting [3]. Many species observed have exhibited type 0 circadian resetting, among them are *Drosophila* [3], humans [28, 38, 53], *Culex* (mosquito) and *Kalanchoe* (plant in succulents family) [54]. The conclusion from these experimental results for modeling is that

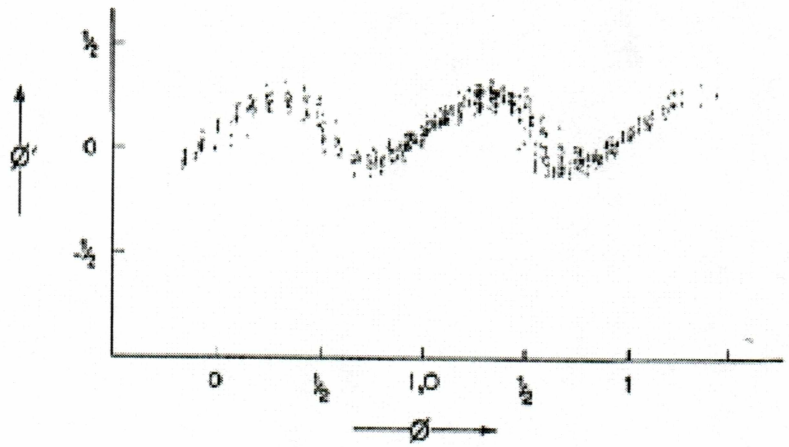

Figure 3.2. Example of a type 0 circadian resetting in *Drosophila*, obtained from 593 eclosion (egg hatching) peaks of populations. The phase $\emptyset'$ after a perturbation by a light pulse is plotted versus the initial phase $\emptyset$ (in units of 24 hours) varying over two days. Type 1 resetting would instead show an averaged slope of 1. Reprinted from Winfree, p.115 [3].

a phase-amplitude oscillator is required to capture the resetting dynamics of a circadian oscillator.

By definition the circadian system is self oscillatory, e.g. it continues to oscillate without external influence (besides those necessary to sustain life). This, combined with the insufficiency of a phase-only oscillator in describing the robustness of phase resetting in circadian oscillators implies that a limit cycle oscillator is required for modeling the circadian system. The van der Pol equation is among the simplest oscillators of this type [12], has been extensively studied analytically [8, 9], numerically [55–57], and it has a history of being used to represent biological oscillators [58, 59]. Goldbeter's biochemical model of the internal workings of fruit fly's circadian system results in limit cycle oscillations [47], providing a molecular basis for our model. A comparison between Goldbeter's model and a van der Pol oscillator shows they have nearly identical dynamical behavior [60]. This, combined with the results from phase resetting experiments and cellular models point to a limit cycle oscillator of the van der Pol type as the most effective way to capture the main dynamics of circadian systems.

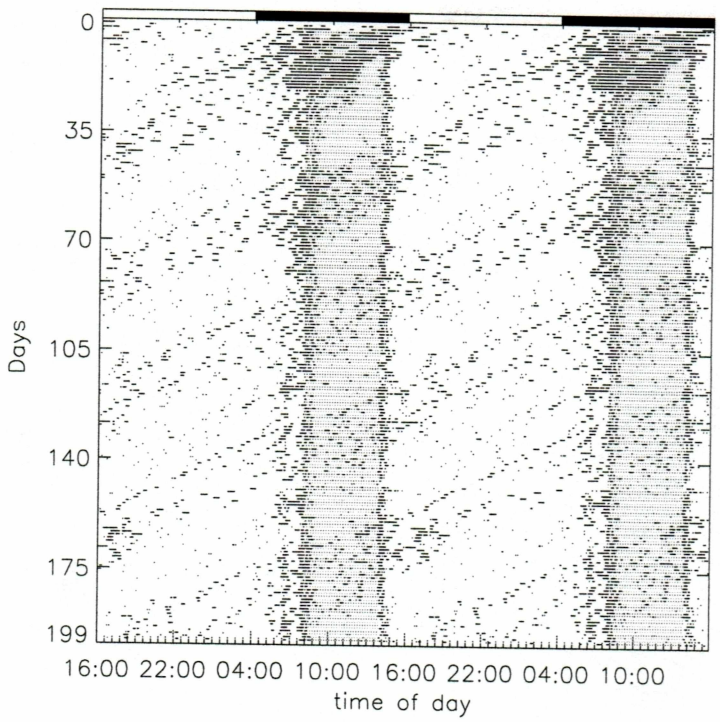

Figure 3.3. Actogram of mouse 1 [1] under food restriction (gray shading indicates availability of food) in a constant dark (DD) environment. Black bars at the top indicate the phase of light immediately prior to this actogram. The mouse exhibits free running behavior with an average period of $\bar{\tau} = 23\,h\,19$ min $\pm\,4$ min, and food entrained behavior with a 24 hour period.

3.2.3 Experiments with Food Restriction and other Zeitgebers

In Figs. 3.3-3.5, three different mice activity patterns are presented exhibiting different behaviors in the presence of a food zeitgeber. The zeitgeber these mice were subjected to consisted of a feeding time restricted to a 6 hour interval each day. A zeitgeber can play an important role in circadian experiments, as it can allow coupled systems that are mutually synchronized to be desynchronized. Czeisler et al. [40] used this technique to desynchronize activity and temperature rhythms in humans in order to measure the period of the 'circadian pacemaker'. By forcing human subjects to have a 28 hour wake-sleep cycle, the period of activity was pulled away from the temperature, melatonin and cortisol cycles, which were unable to synchronize to such a long period. By analogy to the Arnold tongue, where the

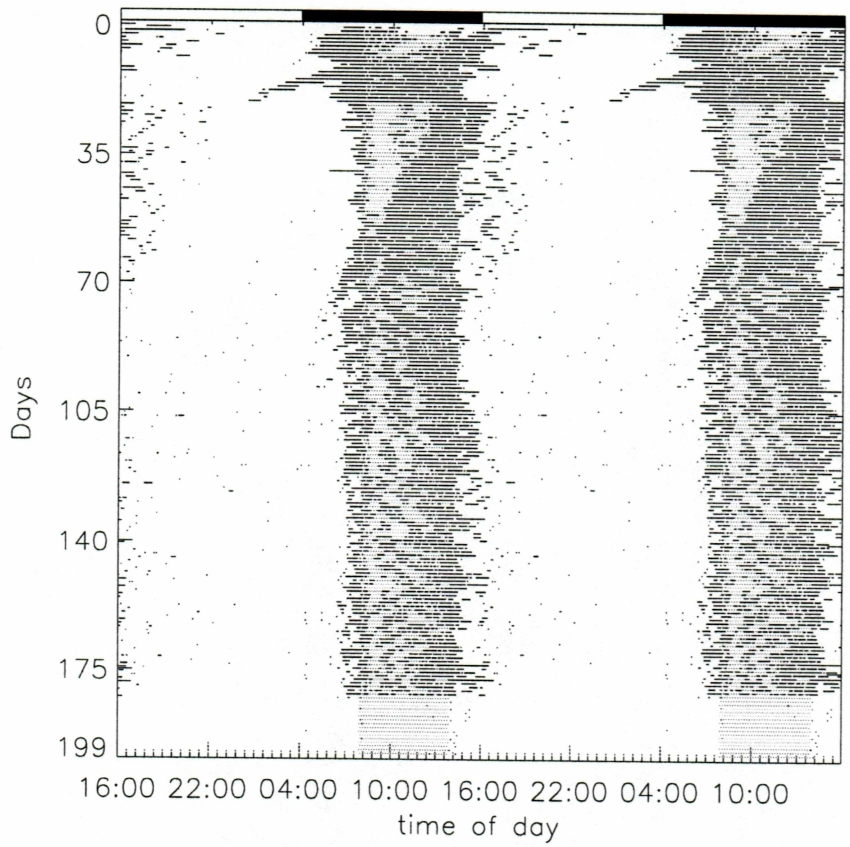

Figure 3.4. Actogram of mouse 2 [1] under food restriction (gray shading indicates availability of food) in a constant dark (DD) environment. Black bars at the top indicate the phase of light immediately prior to this actogram. The mouse exhibits food entrained behavior with a 24 hour period.

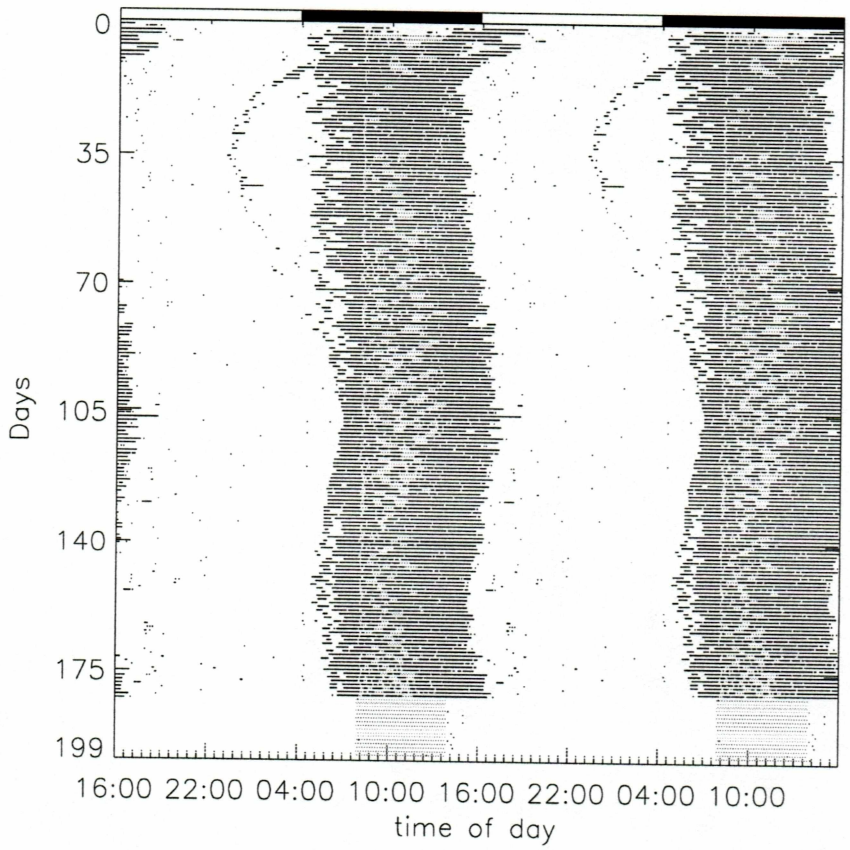

Figure 3.5. Actogram of mouse 3 [1] under food restriction (gray shading indicates availability of food) in a constant dark (DD) environment. Black bars at the top indicate the phase of light immediately prior to this actogram. The mouse exhibits food entrained behavior with a 24 hour period, that appears to be periodically slightly perturbed from a constant phase relation.

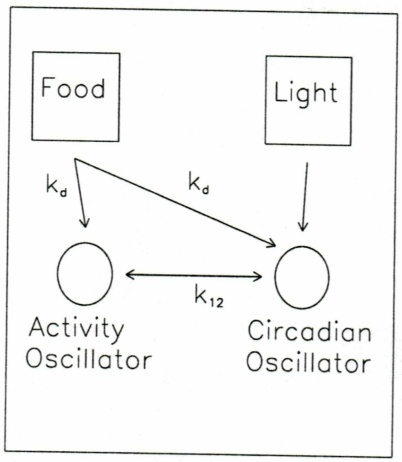

Figure 3.6. Simple schematic of our model. The state of the activity oscillator determines the amount of activity, and the circadian oscillator represents an unspecified background process. Both are driven by the food based zeitgeber and coupled to one another. Kronauer's model [12] utilized a light zeitgeber which only drove the circadian oscillator.

regime of locking is dependent on the detuning $\omega_d - \omega_0$, and the drive coupling k_d, we show in Chapter 3 that if these separate systems have either different 'natural' frequencies or differing levels of susceptibility to a driver, they can be desynchronized by the application of a zeitgeber.

Figure 3.6 depicts a coupled oscillator model, with a light driver that affects the circadian oscillator and a food driver that is coupled to both activity and circadian oscillators. This diagram forms the basis of our model which aims to explain the mice activity data in Figs. 3.3-3.5 where the mice were subjected to a food based zeitgeber. This diagram is the picture of the circadian system that develops from the evidence discussed in the two preceding sections. Observations of internal desynchronization require a minimum of two distinct oscillators to capture the behavior [25], hence the two oscillators labeled, 'Activity' and 'Circadian'. Furthermore, these two oscillators must exhibit limit cycle behavior in order to match the observations of cellular models and phase resetting experiments [3, 50, 51].

3.2.4 Governing Equations

The model we use is a modified version of that used by Kronauer et al. [12] and consists of two driven and coupled Van der Pol (VDP) oscillators (Eqn. (2.1)):

$$\ddot{x_1} - \epsilon(1 - x_1^2)\dot{x_1} + \omega_1^2 x_1 = k_{12}\dot{x_2} + k_{d1} f(t) \tag{3.2a}$$

$$\ddot{x_2} - \epsilon(1 - x_2^2)\dot{x_2} + \omega_2^2 x_2 = k_{21}\dot{x_1} + k_{d2} f(t) \tag{3.2b}$$

where Eqn. 3.2a represents the 'Activity' oscillator and Eqn. 3.2b represents the 'Circadian' oscillator. For $k_{ij} = 0$ these equations reduce to two uncoupled VDP oscillators, as indicated in Eqn. (3.2). Both VDP oscillators are coupled via the velocity with coupling strengths k_{12} and k_{21} respectively. The final term is a time dependent driving term with drive amplitude k_{d1} and k_{d2}. To match the experimental feeding schedule which provided food for six of each 24 hours, we use a squarewave driver,

$$f(t) = H(\sin\omega_d t - \frac{\sqrt{2}}{2}) \quad \text{with } H(x) = \begin{Bmatrix} 0 & x < 0 \\ 1 & x \geq 0 \end{Bmatrix}.$$

This model is designed to be as simple as possible, while capturing the bulk of the behaviors observed in mice. In light of this, we assume that $k_{12} = k_{21}$ and that $k_{d1} = k_{d2} = k_d$.

3.2.5 Relation to the Kronauer Model

Kronauer et al.'s 1982 proposed model [12] (Kronauer's model) was designed to fit observations of the human circadian system, and later modifications improved the fit by adding extra terms to these basic equations. While it included a term to account for a general zeitgeber, in practice Kronauer's model focused on the interaction between light and the circadian oscillator, and it was assumed that the activity oscillator was not coupled to a light zeitgeber.

Kronauer et al also observed that the ratio k_{21}/k_{12} typically had a value of $3 - 5$ in humans [12], putting our assumed ratio of 1 well within an order of magnitude. Forger et al. [44] found that the best fit to human circadian data with a VDP model was with $\epsilon = 0.23$. Furthermore, Forger and Kronauer [60] showed that a method of averaging could be employed to equate their VDP oscillator with a five dimensional, biochemically motivated model [47] of the circadian system of the fruit fly *Drosophila* simply by changing

ϵ to 0.22. Because of this near agreement in ϵ when compared to two very different data sets, it appears that this value of ϵ is universal to animal circadian systems. Therefore, we chose ϵ to be 0.23 because we suspect mice to have a circadian system more similar to other mammals (humans) than to invertebrates and, we know that the model of *Drosophila* is simplified in comparison to the actual biological system.

Chapter 4

Model Behavior versus Experimental Data

4.1 Analysis of mouse activity

In this section we present mouse wheel running activity data collected in the laboratory of Dr. Bult-Ito (Institute of Arctic Biology, Fairbanks, Alaska [1, 7]). Mouse wheel running activity was measured in five minute intervals over a ten month period. Wheel running is a good indicator of the wake-sleep cycle as the majority of an awake mouse's time is spent in the wheel. The original study for which this data was collected [7] consisted of four genetic lines of mice with a total sample size of 105 mice. We present data from 12 of these mice (Appendix A) with activity patterns representative of the entire group.

4.1.1 The training phase

In Fig. 4.1 are activity plots (actograms) of the training phase of three representative mice. The first 107 day training period involved varying conditions. Initially (days 1-21), the mice were given an unlimited supply of food and they experienced 12 hours of light followed by 12 hours of darkness (LD). Mice are naturally nocturnal, so activity and feeding behavior occurs primarily in the period of darkness. On days 22-48 the lights remained constantly off (DD). LD resumed from day 49 through day 107. Beginning on day 56, the mice's food was limited to a weighed amount. Beginning on day 65 the weighed food was available to

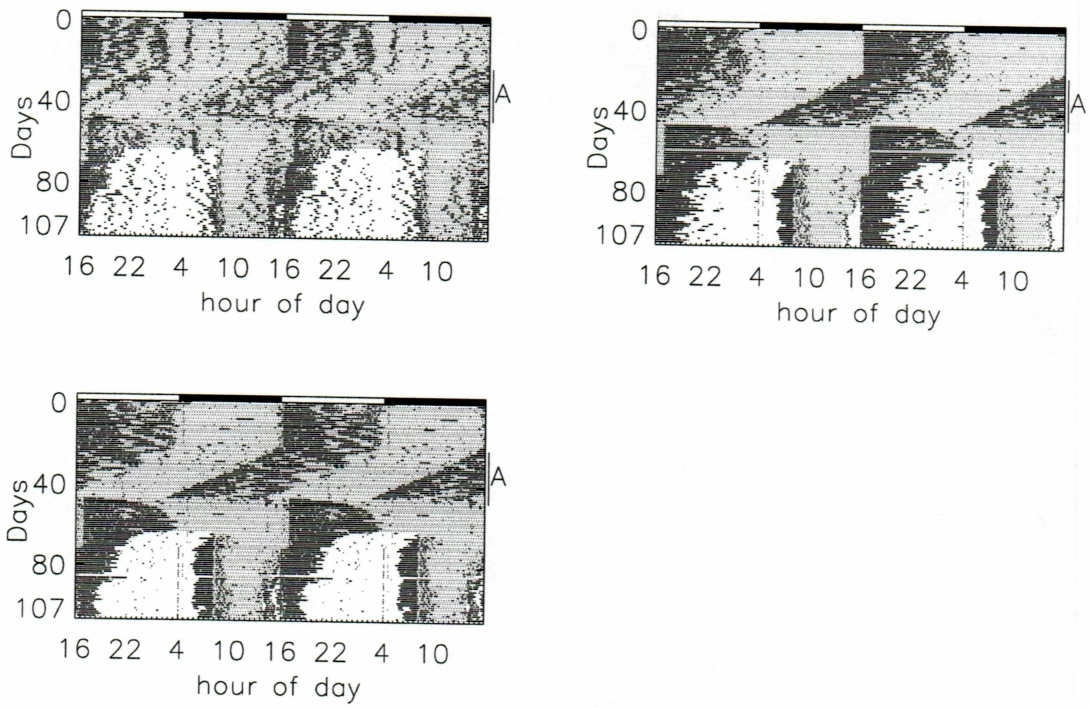

Figure 4.1. Actogram of the training phase for mice 1-3 [1]. All three mice show periods $\tau \approx 23\ h\ 32$ min when not exposed to a zeitgeber (Region A). Actograms show a 48 hour period from left to right, and successive lines are shifted by one 24 hour period in order to provide visual continuity. The legend across the top is broken into 12 hour bands, with black indicating the presence of the light during the training phase. Gray shading indicates the availability of food, and black hashes indicate wheel rotations during a five minute interval. The region marked at right (A) indicates that lights are always off.

the mice for only 10 hours, beginning 2 hours after the lights came on. Beginning on day 72 the weighed food was available only 9 hours, again beginning 2 hours after the lights came on. On days 79, 86, and 93 the times of food availability were successively reduced by an hour. Finally, on day 108, the training phase ended and constant darkness resumed with food available only 6 hours a day. The training phase (Fig. 4.1) results in nearly identical patterns in the period and duration of activity for each mouse: for the first 21 days they all become active at the transition to darkness, following a 24 hour period. Then on day 22 constant darkness (DD) begins, and an external zeitgeber is absent. The mice continue to display periodic activity, *but at a slightly shortened period.* Each day, the mice become

active 20-30 minutes earlier than the preceding day. For 26 days this continues until day 48 (A), at which time mouse 1 and 2 have advanced their subjective mornings by 12h. At the same time, mouse 3 has advanced its subjective morning by about 12h 45 min, slightly more than the other two. Because these mice are receiving no external time signal (light is off) during period A, the periodicity they exhibit must be due to an internal clock. To determine the natural frequencies of the oscillators in our model we use this data interval (A) to measure the average period of the internal clock. Using the onset of activity times, we find that a 12 hour advance in 26 days corresponds to an average daily period that is 28 minutes short of 24 hours (mouse 1 and 2), while mouse 3 is deficient of a full day by 29 minutes. On day 49 the periodic light source is again turned on and the mice resume a 24 hour nocturnal schedule, indicating they are entrained to the period of the external light signal. The 1 hour time shift is due to an error in the protocol. On day 65 at 08:00, food is limited to a 10 hour interval (Fig. 4.1, gray shading), and this interval becomes shorter over the next month. After day 108 when the constant dark (DD) protocol begins and persists through the remainder of the experiment (Region B), the activity pattern of the three mice become very different in behavior (Figs. 4.2, 4.3, 4.4).

4.1.2 Mouse 1: Free Running Behavior

The activity data shown in Fig. 4.2 (region B) exhibits behavior with two distinct periods. 1) Activity due to food availability occurs with a 24 hour period. It starts with a wide band of activity near 07:00 that appears to be synchronized to the feeding times, but that anticipates the food by approximately an hour. It ends with a narrower band that appears when food is removed. Both of these activities occur with a 24 hour period. 2) The second periodicity is due to the rough bands that appear diagonally across the figure with a constant slope. This slope is very close to the slope found in the training phase in the absence of a time signal. We can estimate this period as follows. On day 108 the mouse becomes active around 08:00. Over the next 198 days the start of activity advances in phase by 5 complete days and 16 hours, beginning its final 'day' of activity around 16:00. Allowing for very conservative measurement errors of 6 hours due to the rough nature of the data, we find that the free running period is $23\,h\ 18\ \text{min} \pm 4\ \text{min}$. This free running activity will be the focus of our attention, while the activity synchronized to the food availability in this mouse

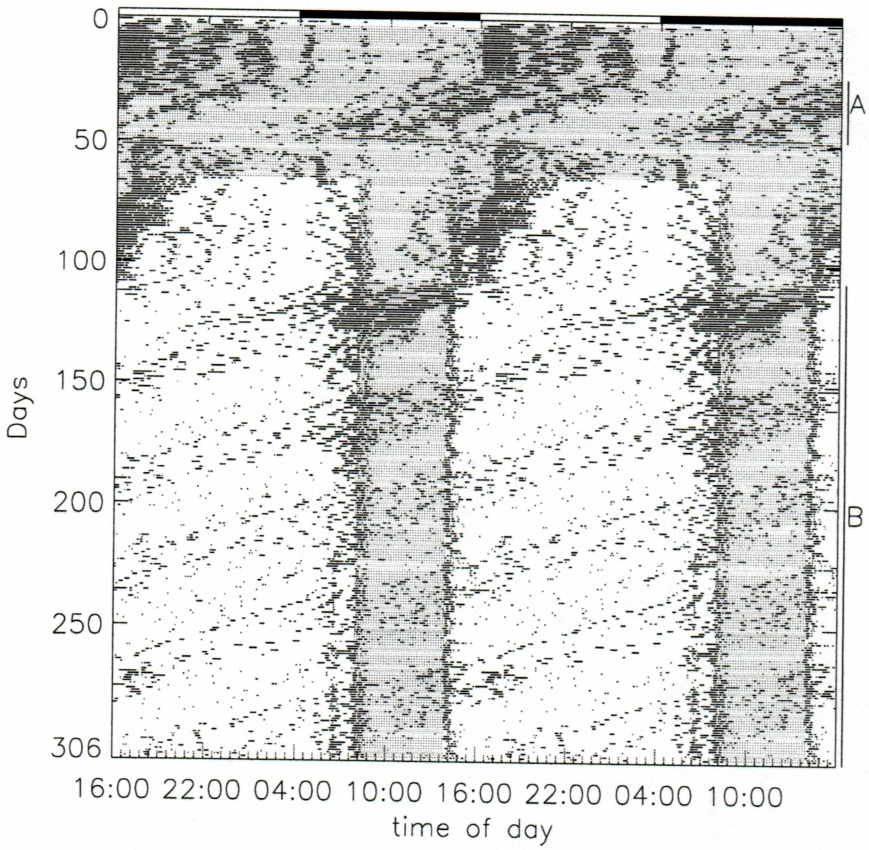

Figure 4.2. Actogram of mouse 1 [1]. During the free running training protocol (A) the mouse exhibits an average free running period $\bar{\tau}_A = 23\,h\,32$ min $\pm$ 5 min. After day 108 (B) the mouse exhibits a free running period $\bar{\tau}_B = 23\,h\,19$ min $\pm$ 4 min. Actograms show a 48 hour period from left to right, and successive lines are shifted by one 24 hour period in order to provide visual continuity. The black bar at the top indicates the timing of lights-on outside of the DD protocol (indicated by regions A and B). Gray shading indicates the presence of food. A black dot indicates more than zero wheel rotations during a five minute interval.

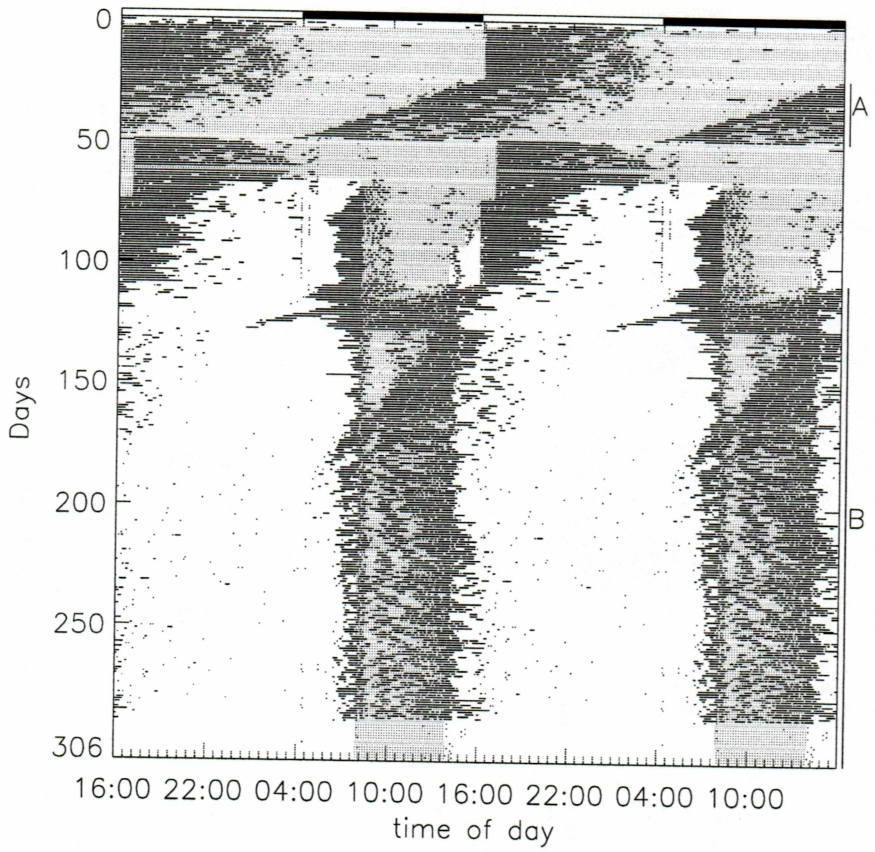

Figure 4.3. Actogram of mouse 2 [1]. After day 108 (B) the mouse exhibits behavior synchronized with food availability. During the training protocol (A) the mouse exhibits a free running period $\bar{\tau}_A = 23\,h\,32$ min $\pm\,5$ min. Refer to Fig. 4.2 for a description.

will not be modeled. Of the 12 mice in our data pool, 5 exhibited behavior nearly identical to this (see appendix).

4.1.3 Mouse 2: Food Synchronized Behavior

In Fig. 4.3 we see some transient behavior between days 108-160 that eventually synchronizes in phase with the food availability from near day 160 through the end of the record. No free running occurs in this data although this mouse expresses an internal period nearly identical to that of mouse 1 during the training period of the mice when no external time signal was supplied. When exposed to the same food zeitgeber their behaviors are entirely different.

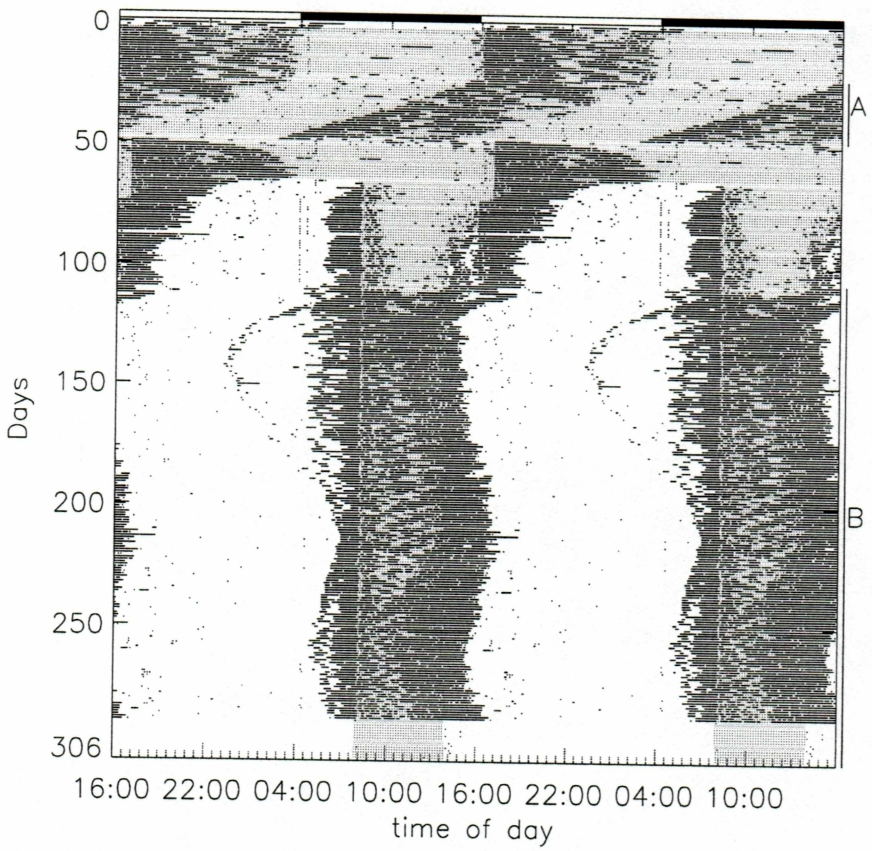

Figure 4.4. Actogram of mouse 3 [1]. After day 108 (B) the mouse exhibits activity behavior synchronized with food availability with a secondary 'beat'. During the training protocol (A) the mouse exhibits a free running period $\bar{\tau}_A = 23\,h\,31$ min $\pm$ 5 min. Refer to Fig. 4.2 for a description.

4.1.4 Mouse 3: Internal Phase Slips?

Similar to mouse 2, mouse 3 (Fig. 4.4) exhibits synchrony of activity with food availability, but superimposed with a secondary 'beat' effect that seems to peak around days 220 and 280, and which perturbs the phase of the mouse activity with respect to the food zeitgeber. This behavior was observed in approximately a third of the 65 mice exhibiting food entrained activity (of 105 total) [61]. Beating effects have also been observed during rodent free running [59, p.84-86].

4.1.5 The question under study

How is it that three mice which exhibit nearly identical natural periods in their activity patterns during the training phase, have such different behaviors when food is restricted? Pavlidis [59] suspected that beating effects he observed under constant dark conditions corresponded to a shift in the periodicity of temperature oscillations. Kronauer [12] proposed a time dependent drift in the natural frequency of his activity oscillator in order to reproduce human activity-temperature desynchronization such as that in Fig. 3.1. This frequency drift resulted in the oscillators transitioning from mutually synchronized behavior, to a phase slipping behavior with respect to one another, which seemed to match the observed behaviors. We ask whether these different mice behaviors can be modeled as different modes of synchronization among the oscillators and driver in our model, without introducing any time dependent frequencies.

4.2 Model Behaviors

We now show how our model can accommodate the above variations of activity behavior and how our model can provide insight into the possible internal clock states of these mice. Because the zeitgeber is food availability, we use a square wave with unit amplitude which is 'on' for 6 of 24 hours. For simplicity we define activity in our model by $x_1 > 0$ (Eqn. (3.2)). We recognize, however, that defining activity by phase rather than amplitude would allow the freedom to choose a relative phase difference between activity and zeitgeber states as has been previously noted [12]. By comparison to a sinusoidal oscillator $x = \sin\phi$, then the range $x > 0$ is equivalent to the domain $\phi \in \big(n\pi, (n+1)\pi\big)$, but nothing demands that this particular range of phases designate activity, merely that the length of the activity interval is approximately half of one full period as seen in the data. So we are free to shift the definition of activity by some constant phase $\phi \in \big(n\pi + c, (n+1)\pi + c\big)$. The cases of driven limit cycle oscillators that we consider will only have small deviations from a limit cycle, so low amplitude oscillations which would be interpreted as unusually short activity intervals will not be a problem for our amplitude definition of activity state. Therefore, our definition of activity is equivalent to a definition based on phase for the parameter regimes of relevance.

4.2.1 A Note on Numerics

To numerically integrate the coupled differential equations (Eqns. (3.2a), (3.2b)) we use a Runge-Kutta scheme with an adaptive step size, which was taken from Numerical Recipies of Fortran [62] and implemented in Interactive Data Language (IDL by RSI). We compared this algorithm with an Euler method and found that the Euler method required stepsizes of $\Delta t = 10^{-4}$ for stability, while the Runge-Kutta used an average stepsize of $\Delta t = 0.39$. On a Dell Precision workstation with 1.3 Ghz Xeon processor with 512 Mb ram this amounted to the Runge-Kutta method being roughly 70 times faster. Partially this speedup is due to inclusion of higher order terms at each iteration which allows larger step sizes while maintaining accuracy. The other part of the time savings came from the adaptive step sizes, which allowed significantly larger steps to be taken in the range $|x_i| \leq 1$ when integrating the VDP equations (Eqns. (3.2a), (3.2b),$|x_i| \leq 2$). The drawback to this was that some stepsizes were so large that they visibly affected the timeseries resolution.

4.2.2 Modes of Synchronization

First we classify the long term behaviors of the activity and circadian oscillators as frequency locked, or not synchronized using the frequency locking criteria defined in Eqn. (2.4) when varying the drive coupling k_d and the coupling between the activity and circadian oscillators k_{12} (Fig. 4.5). Since our model consists of two VDP oscillators and a driver, five modes of behavior are possible.

I. The activity oscillator is locked to the driver, the circadian oscillator is free running.

II. The circadian oscillator is locked to the driver, the activity oscillator is free running.

III. The activity and circadian oscillators are locked both to one another and to the driver.

IV. The activity and circadian oscillators are locked to another, but free running with respect to the driver.

V. The activity and circadian oscillators have periods different from the driver and one another, i.e. no synchronization is present.

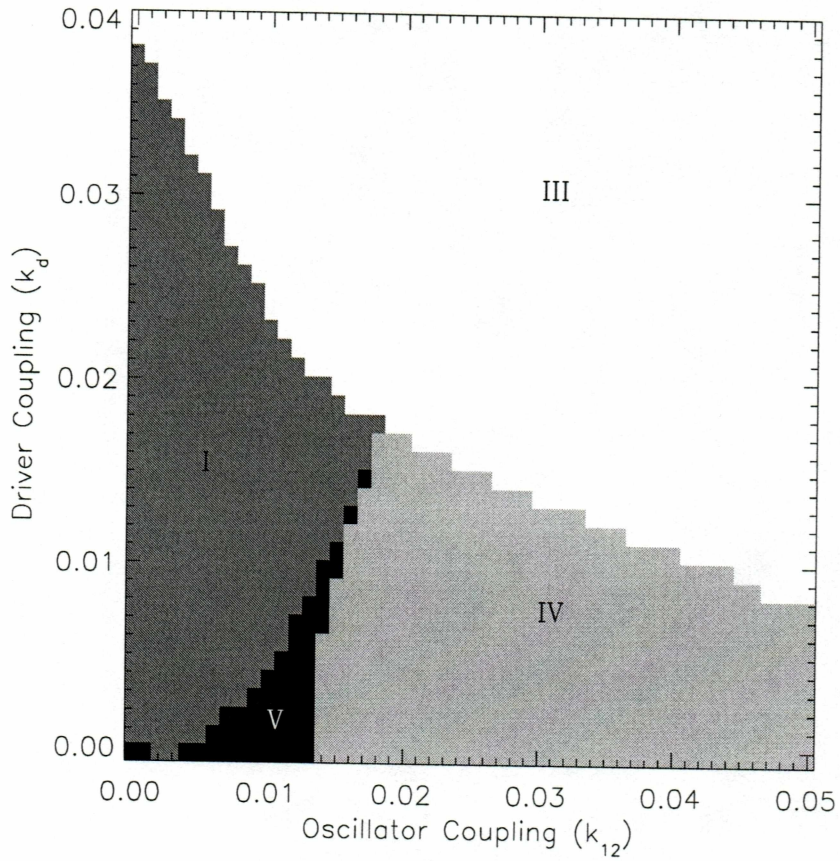

Figure 4.5. A key to synchronization in our model's parameter space (Eqn. (3.2)). The white region corresponds to complete entrainment (III) of the system. Light gray designates the oscillators as mutually synchronized, independent of the driver (IV). Dark gray indicates that the activity oscillator is locked to the driver (I), and black represents the regions of no synchronization (V). Data points were computed at 0.001 intervals along the k_d and k_{12} axes, with $\omega_1 = 0.339$, $\omega_2 = 0.352$ and $\omega_d = 0.330$.

Analyzing Fig. 4.5 we can determine whether the parameter dependance of these five classes of synchronization is intuitive. For the case of no coupling ($k_d = k_{12} = 0$) both oscillators exhibit their individual frequencies, which are different from the driver frequency ω_d. This point in parameter space is indicated as black, which corresponds to no synchronization.

If we keep $k_{12} = 0$ and increase the drive coupling k_d, we expect the oscillators to eventually synchronize with the driver. From our discussion of the Arnold tongue, we

know that synchronization with a single oscillator and driver depends on both the detuning $\omega_d - \omega_0$ and the drive coupling k_d (Fig. 2.6). In this case, the activity oscillator has a smaller detuning than the circadian oscillator, so it is expected that it would synchronize to the driver with a weaker drive coupling than needed to synchronize the circadian oscillator. This is confirmed in the map which shows that with $k_{12} = 0$, the activity oscillator locks to the driver for $k_d \geq 0.001$ and the circadian oscillator also locks to the driver (and to the activity oscillator by default) when $k_d \geq 0.038$.

Alternately, if we fix $k_d = 0$ and increase k_{12} from zero we see that for sufficiently large coupling the two oscillators lock to a frequency independent of the driver. But something unexpected happens at $k_{12} = 0.002$, where the activity oscillator is synchronized to the driver. In Fig. 4.5 the natural frequencies ω_1 and ω_2 are each always larger than the drive frequency ω_d. However, when these oscillators are in isolation ($k_d = k_{12} = 0$) a different story is told (see Figs. 4.6, 4.7). Figure 4.6 shows that the observed frequency of our activity oscillator is actually slightly less than the drive frequency ω_d, while Fig. 4.7 depicts our circadian oscillator with an observed frequency greater than ω_d as expected. When we first introduced the VDP equation (Eqn. (2.1)) we mentioned that the observed frequency was not identical to the natural frequency ω_0 (for $\epsilon > 0$) due to the nonlinear term, and here we show evidence of that. As k_{12} is increased, the observed frequencies of the activity and circadian oscillators adjust towards one another. The unexpected locking of the activity oscillator to the driver near the point ($k_{12} = 0.002, k_d = 0$) in parameter space is the result of the shift in the activity oscillators frequency caused by the circadian oscillator, such that the observed frequency of the activity oscillator is indistinguishable from the frequency of the driver.

4.2.3 Recreating the Experimental Data

In order to locate the region of parameter space that will best mimic the mice activity patterns, we review the relevant information. All three experimental mice data show a period of about 23.5 hours in the absences of any external time signal during the training phase (Figs. 4.2-4.4, region A). It is believed [12, 25] that this behavior corresponds to the activity and circadian oscillators being synchronized but free running with respect to the drive. In Fig. 4.5 this condition is met in the light gray parameter range in the absence of

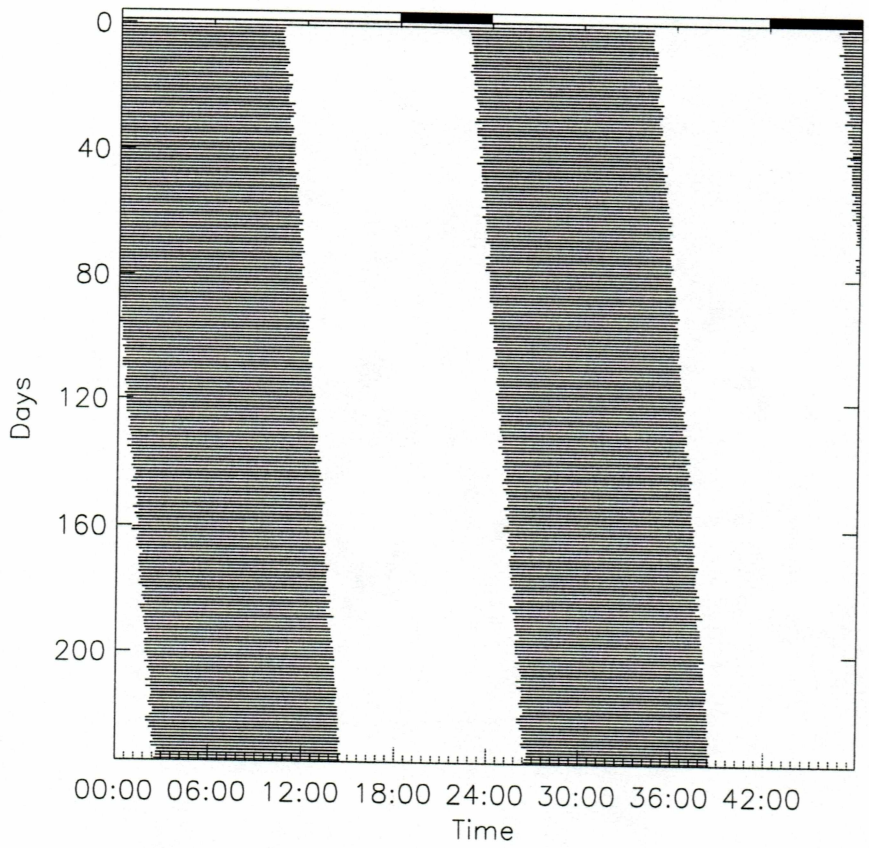

Figure 4.6. Actogram generated by the activity VDP oscillator ($x_1 > 0$ Eqn. (3.2a), black) in isolation from the driver and the circadian VDP oscillator. The legend across the top indicates the period of the driver. $k_d = k_{12} = 0$, $\omega_1 = 0.339, \omega_d = 0.330$.

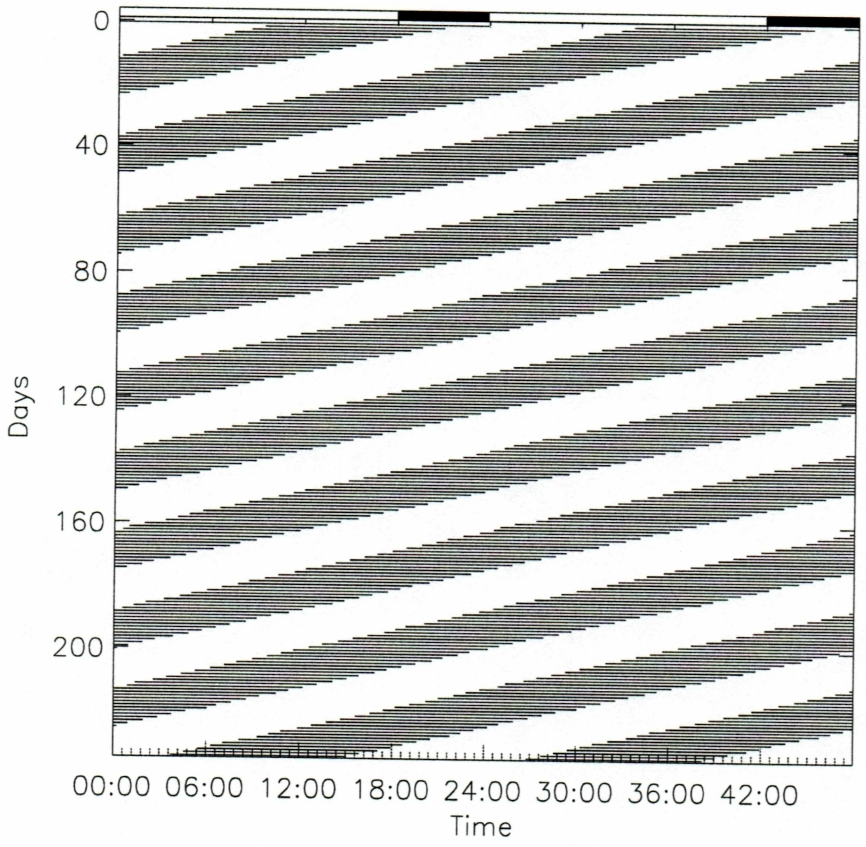

Figure 4.7. The activity of the circadian VDP oscillator ($x_2 > 0$ Eqn. (3.2b), black) in isolation from the driver and the activity VDP oscillator. The legend across the top indicates the period of the driver $k_d = k_{12} = 0$, $\omega_2 = 0.352, \omega_d = 0.330$.

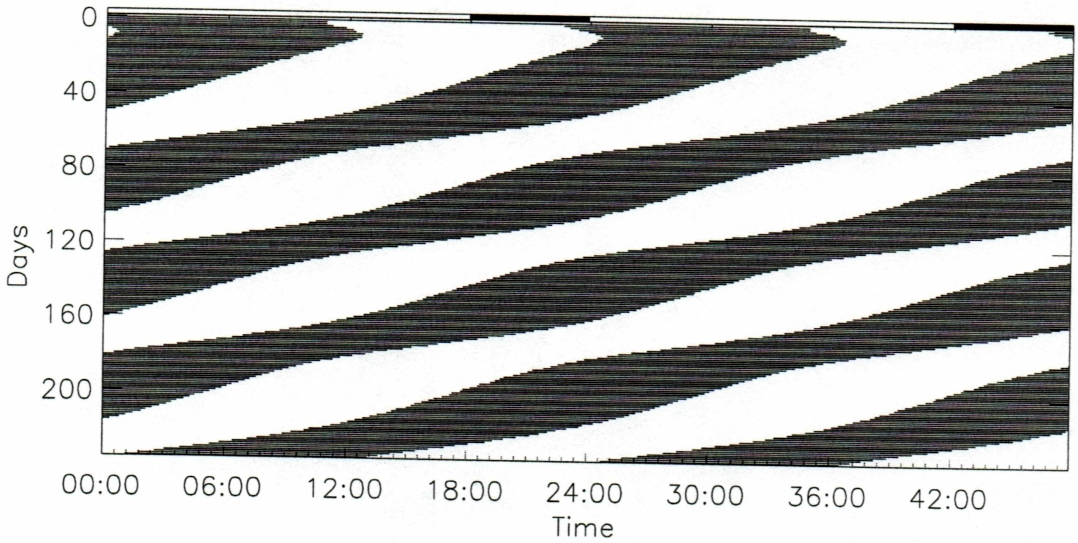

Figure 4.8. Actogram of mouse 1 type behavior produced by our model (Eqn. (3.2)). $k_d = 0.006$, $k_{12} = 0.014$, other parameters are the same as in Fig. 4.5. The average period of this behavior is $\bar{\tau} = 23\ h\ 24$ min, as compares to $\bar{\tau}_B = 23\ h\ 19$ min $\pm$ 4 min in the experimental mice data (Fig. 4.2). The legend along the top shows food availability in black.

a zeitgeber ($k_d = 0$). By subjecting the three mice to a food zeitgeber ($k_d \neq 0$), different types of activity are evoked. If this external signal is the primary cause of the observed differences in behavior, than could it be that the differences are caused by a different level of sensitivity to this food zeitgeber in each mouse?

For the experimental actograms we only attempt to reproduce experimental activity from day 108 onward, so a roughly 200 day interval is plotted to compare to the last 200 days of the actograms in Figs. 4.2-4.4. Initial conditions are of little importance, as asymptotic phase relations are governed mainly by frequency relationships, with the exception of the black region in Fig. 4.5 where the system components interact in very complex ways. In Fig. 4.8 we demonstrate behavior of the free running type observed in mouse 1 (Fig. 4.2). In our map of parameter space (Fig. 4.5), this free running actogram would be situated near the lower left of the light gray region, identified with activity and circadian oscillators being synchronized independent of the driver. The actogram in Fig. 4.9 is representative of frequency locking between the activity oscillator and the zeitgeber (Eqn. (2.4)) shown

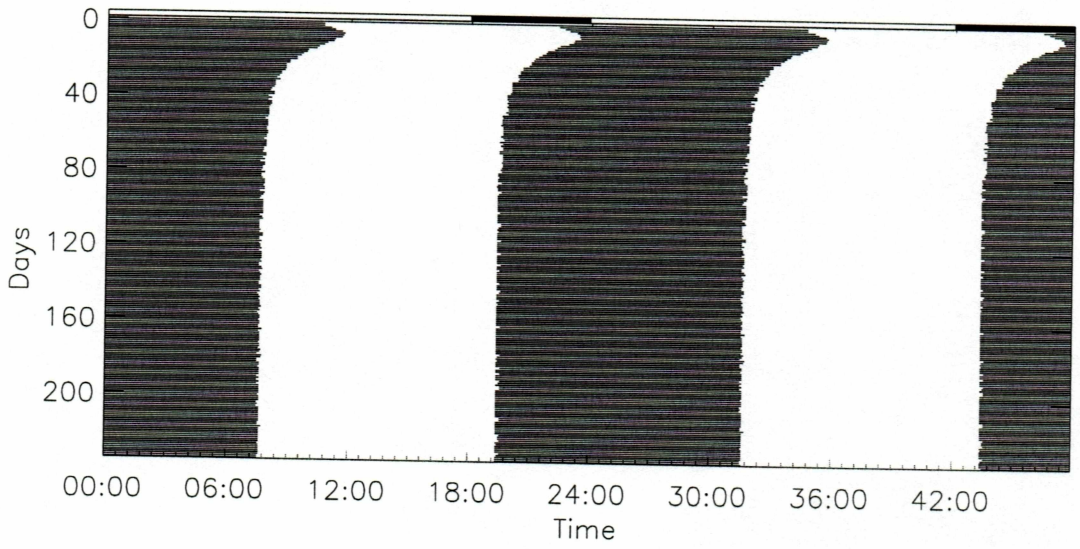

Figure 4.9. Actogram of mouse 2 type behavior produced by our model (Eqn. (3.2)). $k_d = 0.022$, $k_{12} = 0.014$, other parameters are the same as in Fig. 4.5. Food availability is represented by a black bar in the legend at top. Compare to the experimental data in Fig. 4.3.

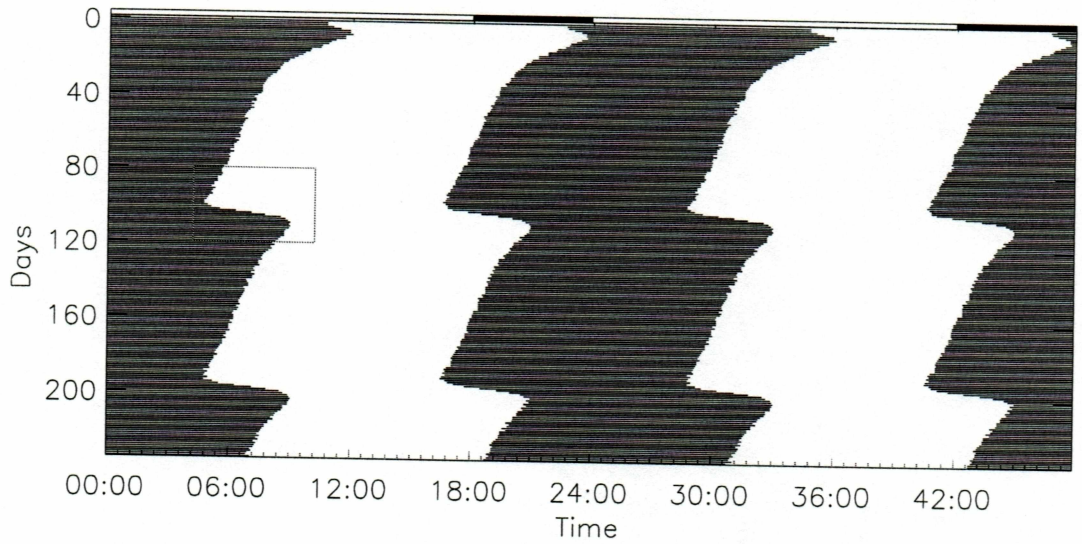

Figure 4.10. Actogram of mouse 3 type behavior produced by our model (Eqn. (3.2a)). Perturbation noted in the figure corresponds to the phase slip in Fig. 4.11. $k_d = 0.0188$, $k_{12} = 0.014$, other parameters as in Fig. 4.5.

by mouse 2 in Fig. 4.3. This modeled actogram is located in the white region of Fig. 4.5 which indicates both oscillators are synchronized to the driver. The only parameter changed between Figs. 4.8 and 4.9 is the driver coupling coefficient, which is about four times larger than for the free running behavior modeled after mouse 1.

Figure 4.10 demonstrates beating effects of the type observed for mouse 3 in Fig. 4.4. Here the activity oscillator is locked to the driver while the circadian oscillator (Fig. 4.11) is near the boundary of an Arnold tongue and occasionally makes rapid phase slips. These phase slips cause the perturbation of the activity oscillator (near days 120 and 200), resulting in the aforementioned 'beating' effect. While Fig. 4.10 displays periodic perturbations and can also explain the observed activity period during the training phase, its activity profile is much more abrupt than that of mouse 3 (Fig. 4.4). In Fig. 4.12 we show that a small variation of k_{12} can produce a much smoother activity profile, such that the perturbations occur in less abrupt fashion. In the parameter map (Fig. 4.5) beating behavior is produced in the dark gray region due to phase slips of the circadian oscillator.

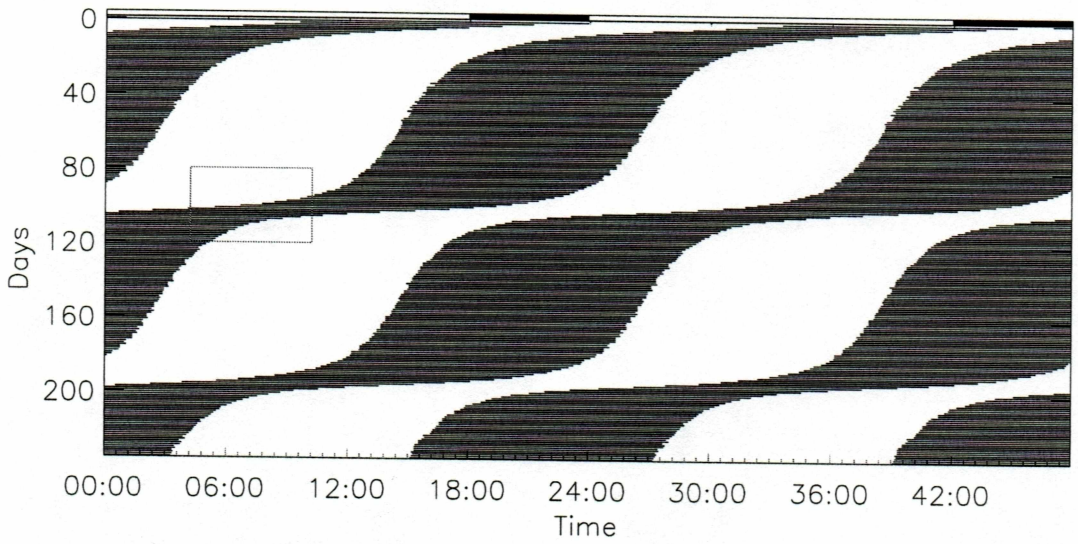

Figure 4.11. The behavior of the circadian oscillator ($x_2 > 0$ Eqn. (3.2b), black) when the activity oscillator shows beating (Fig. 4.10). Phase slip noted in the figure corresponds to the perturbation in Fig. 4.10. $k_d = 0.0188$, $k_{12} = 0.014$, other parameters as in Fig. 4.5.

4.2.4 Model Validation

Finally, we make a quantitative comparison (Figs. 4.13, 4.14) between the model and experimental data by plotting the phase difference between each activity oscillation and the food zeitgeber. For the experimental data, phase was determined by identifying the midpoint of each interval of activity. By using a moving average to smooth the binary data a peak resulted near the center of each cluster of activity. This phase of this peak was used as the representative phase for that 'circadian days' activity. Using a single point per day is equivalent to the 'uniform phase measure' defined in section 2.1.5. We see that the average period of the free running mouse (Fig. 4.2, $\bar{\tau}_B = 23\,h\,19$ min $\pm\,4$ min) is somewhat shorter than the average period of its mathematical analog (Fig. 4.8, $\bar{\tau} = 23\,h\,24$ min) as indicated by the different slopes. Both the food entrained mice and models (Fig. 4.14) exhibit the expected 24 hour period, and the perturbation in the modeled data occurs at approximately the same time (both have local phase minimums near period 105) as in the experimental data. Furthermore, the experimental data appears to be undergoing a second perturbation

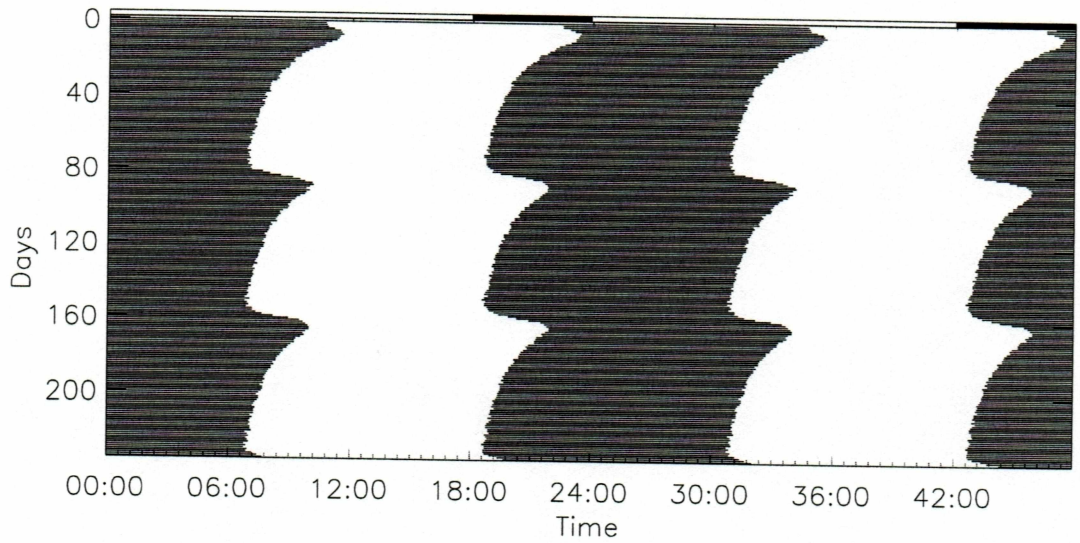

Figure 4.12. Actogram of mouse 3 type behavior produced by our model (Eqn. (3.2)), with an activity profile that appears more similar to the behavior shown in Fig. 4.4. $k_d = 0.050$, $k_{12} = 0.011$, other parameters as in Fig. 4.5

at the end of the data series, and the model is approaching a second perturbation. In the model, these perturbations are the result of the circadian oscillator undergoing a phase slip in relation to the driver and the activity oscillator. This comparison provides evidence that the biological system is being perturbed by an internal phase slip. By analogy to existing data in humans, we suspect that the phase slips will be observable in mouse body temperatures taken during similar perturbed wheel running activity patterns.

All three of the mice we are modeling exhibit a nearly identical activity period in the absence of an external time signal during the training phase. The condition of no zeitgeber is equivalent to setting the drive coupling (k_d) to zero. Since the model actograms in Figs. 4.8-4.10 all share the same coupling k_{12}, projecting their location in Fig. 4.5 down to the horizontal axis gives the same point in our parameter space and the resulting behavior with average period $\bar{\tau} = 23h37$ min is shown in Fig. 4.15. This is comparable to the average period $\bar{\tau}_A = 23\ h\ 32\ \text{min} \pm 5\ \text{min}$ observed in mice 1-3 (mouse 3 has a 1 minute shorter period).

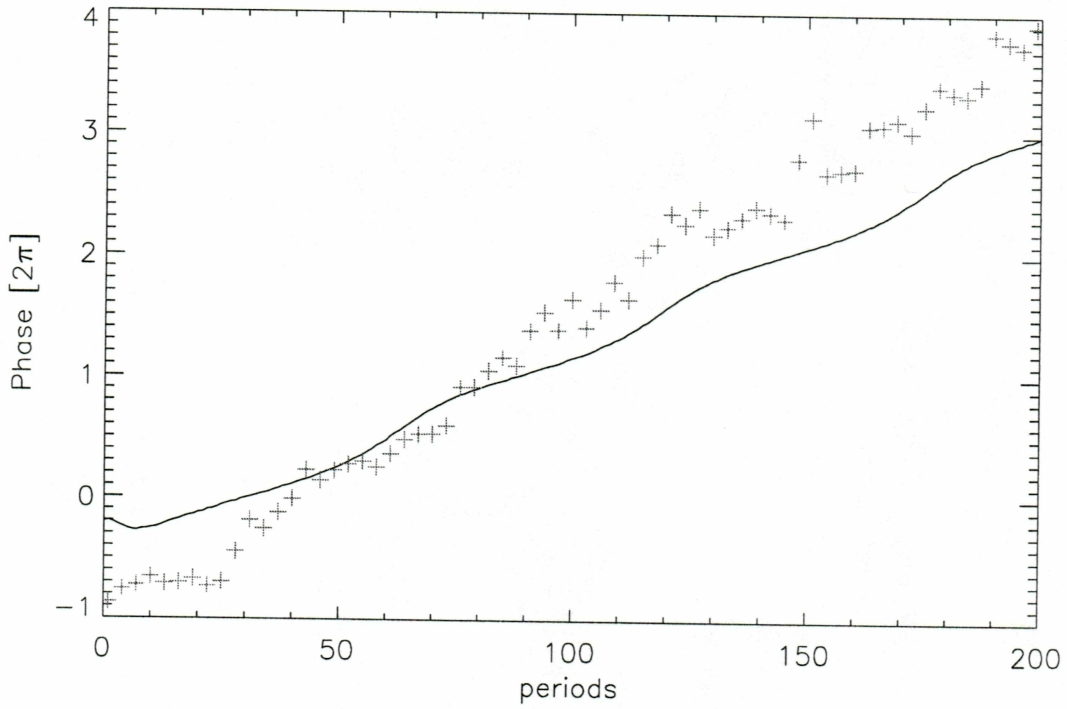

Figure 4.13. Comparison between the experimental (gray crosses) and modeled (black line) activity-driver phase difference in the free running mouse. Figs. 4.2 and 4.8, respectively.

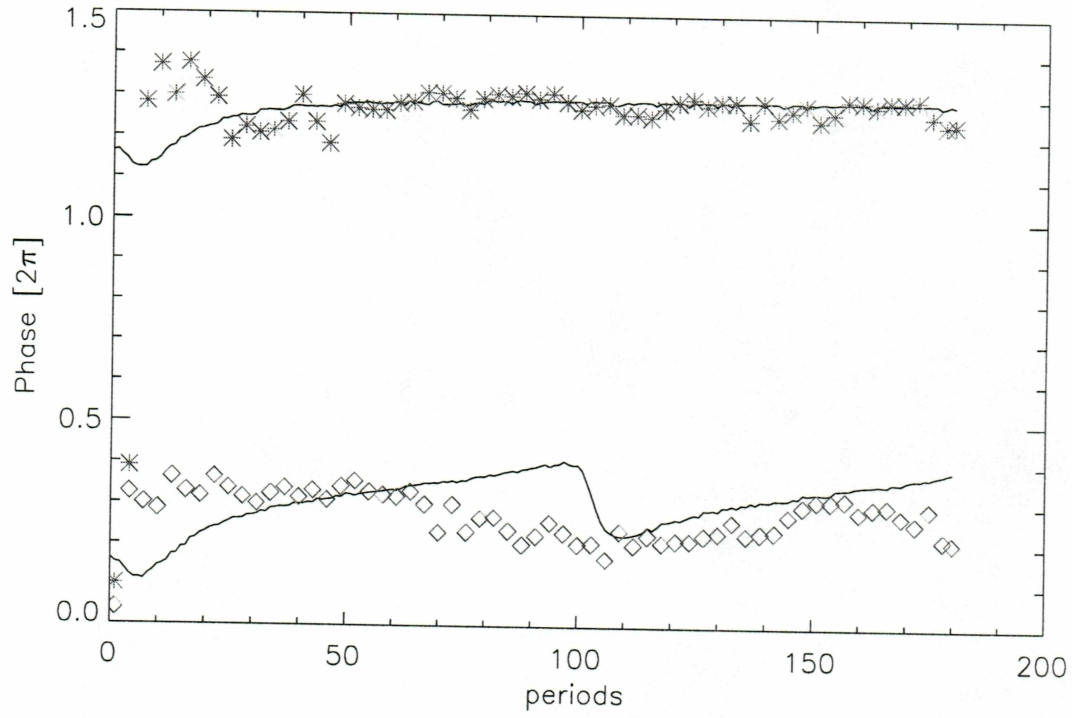

Figure 4.14. Comparison between the experimental (gray points) and modeled (black lines) activity-driver phase differences in the food entrained mice. Asterisks and solid line represent the frequency locked behavior in Figs. 4.3 and 4.9. Diamonds and corresponding line shows the perturbed behavior shown in Figs. 4.4 and 4.10. Each experimental phase represents the average of three successive data points for clarity. Phase of the modeled behaviors have been shifted by a constant to align with the experimental data.

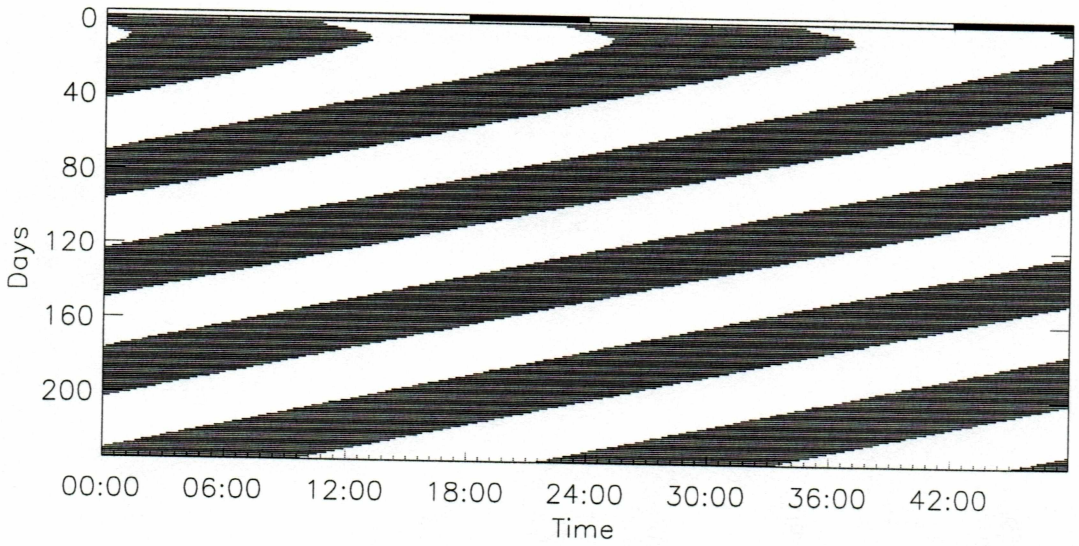

Figure 4.15. Actogram of model behavior in the absence of a zeitgeber. This modeled system exhibits an average period $\bar{\tau} = 23\,h\,37$ min, which is comparable to the experimental training period of $\bar{\tau}_A = 23\,h\,32$ min $\pm\,5$ min. $k_d = 0.000$, $k_{12} = 0.014$, and other parameters as in Fig. 4.5.

4.2.5 Alternative Coupling Topologies

In the model discussed to this point (Fig. 3.6) we have assumed that the drive is coupled to both the activity and the circadian oscillator, while the Kronauer model for a light stimulated zeitgeber had only the circadian (Kronauer et al. [12] identified it as 'temperature') oscillator being effected by the driver. Is this driver coupling to both oscillators necessary, or could a connection topology similar to that of the Kronauer model be sufficient to explain the mice activity? In Fig. 4.16, we show the $k_d - k_{12}$ parameter space for a modified model (Eqn. (3.2), $k_{d1} = 0$, $k_{d2} = k_d$) in which the driver is coupled to the circadian oscillator but not directly coupled to the activity oscillator. With no coupling to the driver ($k_{d1} = 0$), the activity oscillator can still synchronize to the driver through perturbations transmitted through the circadian oscillator (see [52] for a similar effect) except for $k_{12} = 0$ when the activity oscillator cannot synchronize with the driver or the circadian oscillator. We also see from Fig. 4.16 that for no k_{12} value do the three required synchronization conditions coexist to recreate the three different mice behaviors while at the same time expressing equivalent periods in the undriven case. Mouse 3, with its activity oscillator synchronized to the drive, and the circadian oscillator nearly synchronized with intermittent phase slips that perturb the activity oscillator cannot be modeled to match both the experimental training phase (region A) and the experimental food entrained (region B) behaviors (Fig. 4.4). The dark gray region of Fig. 4.16 corresponds to the mode of synchronization needed to reproduce the 'beating effect', but for any value of k_{12} in this region, when k_d is set to zero to compare with the undriven training phase case the activity oscillator will fail to synchronize to the circadian oscillator. This synchronization failure will result in a significant difference between the experimental and the modeled undriven activity period.

Similar to the previous key (Fig. 4.16), Fig. 4.17 shows that the three synchronization conditions are not met for a single coupling strength k_{12} when the driver is only coupled to the activity oscillator (Eqn. (3.2), $k_{d2} = 0$). Because disabling one of the oscillators destroys the conditions necessary to recreate the experimental data, this provides evidence that a food based zeitgeber interacts with each oscillator.

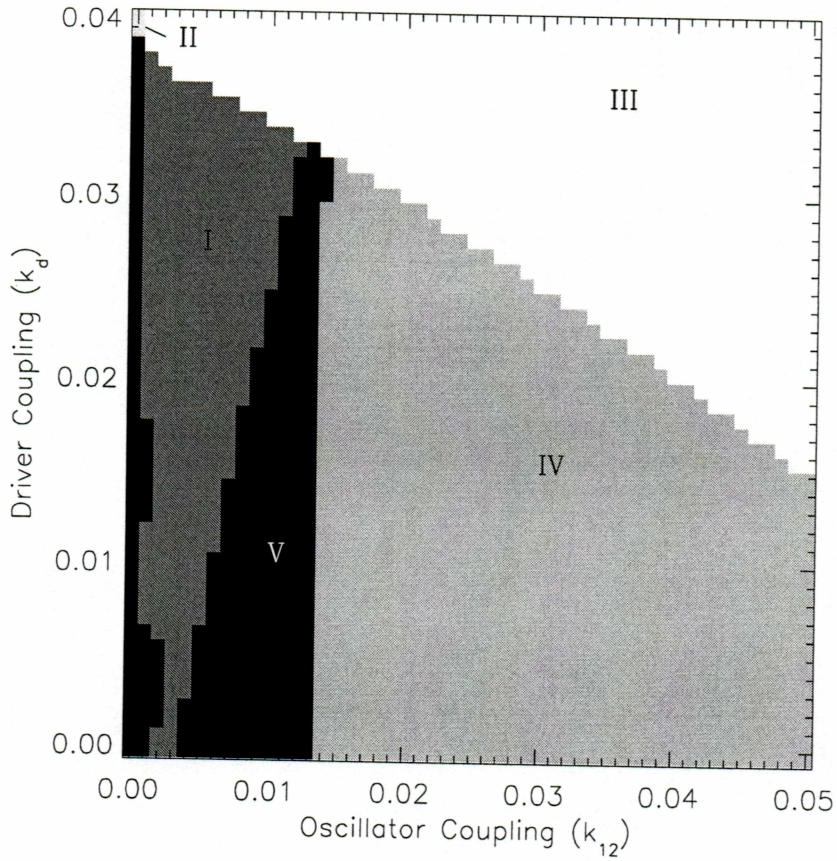

Figure 4.16. A key to synchronization types in $k_d - k_{12}$ parameter space with no drive coupling to the activity oscillator ($k_{d1} = 0$ in Eqn. (3.2a)). The white region corresponds to complete entrainment (III) of the system. Light gray designates the oscillators as mutually synchronized, independent of the driver (IV). Dark gray indicates that the activity oscillator is locked to the driver (I), and black represents the regions of no synchronization (V). The light gray in the upper left corner (II) indicates that only the circadian oscillator is locked to the driver. Other parameters are the same as in Fig. 4.5.

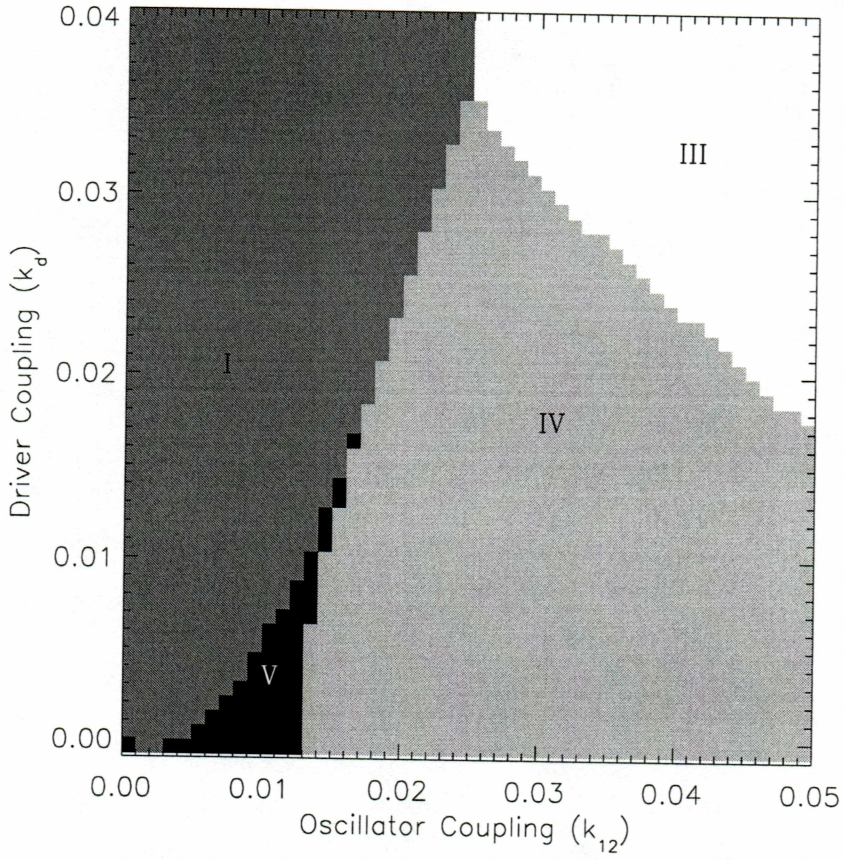

Figure 4.17. A key to synchronization types in $k_d - k_{12}$ parameter space with no drive coupling to the circadian oscillator ($k_{d2} = 0$ in Eqn. (3.2b)). The white region corresponds to complete entrainment (III) of the system. Light gray designates the oscillators as mutually synchronized, independent of the driver (IV). Dark gray indicates that the activity oscillator is locked to the driver (I), and black represents the regions of no synchronization (V). Other parameters are the same as in Fig. 4.5.

Chapter 5

Discussion

In the previous chapter, we showed that a simple model (see Fig. 3.6, Eqns. (3.2a) and (3.2b)) consisting of two coupled oscillators can explain much of the rhythmic circadian behavior observed in food entrainment studies of mice. Using van der Pol oscillators to represent an 'activity' oscillator that generates overt behavior, and a 'circadian' oscillator that influences the activity oscillator, we relate various mouse activity patterns to different modes of interaction between our two oscillators and a driver (zeitgeber). These different modes are explained in relation to Arnold tongues, which are mathematical structures in parameter space that determine the degree of synchronization between a driver and an oscillator as a function of relative frequencies and coupling strength. We now provide some understanding of how this model might be interpreted in terms of biological knowledge.

5.1 Applications in Biological Systems

Previous studies in humans found that a similar model's equivalent of our circadian oscillator is correlated with body temperature [12]. Lesioning studies have indicated that body temperature is controlled in the suprachiasmatic nuclei (SCN) [37], which means that our circadian oscillator may represent the collective output of the SCN.

It is known that temperature oscillations are not equivalent to the chemical oscillations within the SCN, as temperature is dependent on activity and food intake. Temperature may also provide feedback, possibly affecting the rate of transcription of PER type proteins

that are the molecular basis of circadian rhythmicity. In mammals, physical destruction of the SCN eliminates rhythmicity in body temperature and activity when subject to a light zeitgeber or in the absence of any zeitgeber [29, 31, 37, 63] . However, when subjected to a food zeitgeber, rats are able to synchronize to food availability and exhibit activity before the expected appearance of food [37]. This may imply that there is some pacemaker outside of the SCN that is capable of entraining to food availability. Several different studies have found evidence that circadian oscillators in peripheral systems such as the liver, kidney, or pancreas will entrain to a food zeitgeber under both LD (typical day-night light cycles) and DD (constant dark) conditions, but that these peripheral systems are unable to entrain the rhythmic expression of PER proteins in the SCN within one week [36]. A longer term study of mice (conducted by our collaborators) has found that a food zeitgeber administered under DD conditions can entrain expression of PER in the SCN, but that it takes approximately 12 weeks [7]. This is a strong indication that light acts as a much more potent zeitgeber than food availability, as light will fully entrain most subjects within a few days. Mistlberger has done many experiments trying to locate a food entrainable pacemaker in the brain or in peripheral systems but has not identified any single system as the locus [64].

One drawback of using PER proteins as an indicator of the SCN state is that measurement requires sections of the SCN, effectively removing the subject from the experiment for a single data point. Comparisons are made by finding animals that display similar actograms, and then measuring the PER concentration from different animals at different phases of activity. Because of this, most studies take relatively few PER samples over one cycle, often about six samples each day [7, 36]. Studies of SCN cells maintained in a culture have measured electrical potentials which show patterns of neuron firings [50, 65] with peaks in firing activity with a circadian period. The firings of individual cells do not appear to be synchronized [65], though the mean period of all cell firing rhythms agrees with the circadian period of the animal from which the cells were taken [50]. The studies analyzing PER concentrations in the SCN show that many of the cells are synchronized [7, 36], and it seems that this is the result of coupling among cells [66] rather than due to the influence of a zeitgeber which synchronizes each cell individually. From a physical viewpoint, the synchronization of SCN cells in the absence of any external time signal seems sufficient evidence for coupling among cells, whether direct or circuitous. Also not determined in

biological research is the extent to which PER concentration, neural firing patterns, body temperature and other measures of circadian rhythmicity are related.

Based on this information, it is impossible to say that the oscillator we name 'circadian' represents any one of these indicators of circadian rhythmicity. Our model is aimed to simplify a very complex system, and this was one trade-off made in exchange for clarity. The comparison done between the van der Pol oscillator and Goldbeter's model [47] of protein transcription did not equate the dynamical variables of the VDP oscillator to any single dynamical variable in Goldbeter's model [60]. Instead, the two dynamical variables of the VDP oscillator were shown to align with a generalized coordinate system constructed from the five dynamical variables in Goldbeter's model, which represented concentrations of various PER proteins. The VDP oscillator captured the most essential behavior while eliminating three dynamical variables, but these two variables could no longer be interpreted as a single chemical concentration. Likewise, our circadian VDP oscillator may represent some combination of the commonly measured variables of SCN state.

Recent studies of *Drosophila* have found individual collections of cells that control activity in relation to light onset, and a separate group of cells that control activity in relation to the onset of dark [2]. *Drosophila* does not possess a structure as specialized as the mammalian SCN, so it is difficult to make comparisons, but the SCN does have two distinct lobes. It has been reported that the cells in these lobes can be synchronized in an anti-symmetrical arrangement under normal conditions [67]. This may be the physical location of our 'activity' oscillator. However, this implies that destruction of the SCN should eliminate all periodic activity, which is not the case when SCN-ablated animals are subjected to a food zeitgeber [31]. More likely, our activity oscillator does not correspond to any particular collection of cells, but serves as a convenient replacement for many diverse systems that contribute to activity.

Careful observation of our model actograms will show that the phase of modeled activity relative to the food zeitgeber does not agree with that seen in the mouse data. We addressed this earlier in section 4.2, by stating that we can easily redefine 'activity' by phase rather than amplitude, allowing us to shift the phase by any constant. If temperature or another measure of circadian state where collected in addition to activity data, a good test of our model would be to determine whether this data was strongly correlated with our 'circadian' oscillator, within a constant phase.

5.2 Applications in Nonlinear Dynamics

By analogy to the understanding of coupling among general nonlinear oscillators [51, 52, 68], we can make a general statement about coupling between cells expressing periodic behavior. It should be stressed that the 'intrinsic' period τ_0 of a cell is the period it will exhibit in isolation from all other effects. When part of a coupled population of cells, the same cell will exhibit some modified period τ_{eff}, which is dependent on the strength of the coupling and the relation between the diverse periods of the cell population and τ_0. For weak coupling, $\tau_{eff} \rightarrow \bar{\tau}_0$ as the coupling becomes sufficiently strong to synchronize, meaning that the individual cells will adjust their periods towards the mean period $\bar{\tau}_0$ of the population. For strong coupling this is not necessarily true. Under strong coupling, the synchronized period could be smaller or larger than every individual period τ_0.

Knowledge provided by this study may be of interest in more general experimental and theoretical studies. Consider two systems that are observed to oscillate in synchrony. It could be that they are fully independent systems, capable of oscillating independently, that are coupled together with sufficient strength so that their individual intrinsic frequencies adjust to some mutual frequency (e.g. two nonlinear springs). Alternatively, it could be that they have the same frequency of oscillation because one system lacks an intrinsic ability to oscillate independently and is only responding to a driving force (e.g. spring and mass). If we are able to drive both systems, then by carefully adjusting the frequency of the driver we can decouple the two independently oscillatory systems by synchronizing *either* one of the oscillators to our driver, while the other oscillator continues to oscillate independently. However, in the second case our driver could synchronize with the mass while the spring oscillates independently, but if the spring is synchronized to the driver the mass must be synchronized also. This allows us to determine the properties of our two systems. For difficult to isolate systems, such as are common in biology, this may be the only practical way to learn whether a system is intrinsically oscillatory in nature.

The single driven van der Pol oscillator contains a rich bifurcation structure with period doubling cascades, devil's staircases and chaotic attractors [69]. By classifying the behavior of our model (two coupled and driven VDP oscillators) into different modes of synchronization, we have undertaken a very preliminary bifurcation study of this very complex system.

The boundary of an Arnold tongue corresponds to a saddle-node bifurcation [69]. Therefore, the boundaries between different modes of synchronization in our keys of parameter space (Figs. 4.5, 4.16, 4.17) indicate saddle-node bifurcations in this region of parameter space. The black region (no synchronization) in these keys exhibited very interesting quasi-periodic behavior that appears to be a reflection of the three different periodicities present in the system, though further study is merited.

5.3 Future Studies

Other interesting possibilities for further research may lie in a cellular model (as in Eqn. (3.1)) of synchronization in the circadian system. One unsurprising weakness of our current model is its inability to produce the feeding behavior in the free running mice (as in Fig. 4.2), because each oscillator has one fundamental frequency that it displays. A simple modification of the present model to reproduce both the feeding and the free running behavior would involve adding an additional oscillator, which would make the model more complex while adding a little explanatory power. This process of adding oscillators could be repeatedly applied to explain lower order effects, essentially becoming a power series expansion. This seems to violate our original motivations of maximizing simplicity for maximal understanding. It would be interesting to see whether a simple Gaussian distribution of cell frequencies, when weakly coupled together and driven at a frequency near the mean, would produce a bimodal frequency distribution to represent the free running period and the 24 hour 'feeding period'. The analogy to our free running mouse behavior should be evident, though how well the analogy will stand under scrutiny is not clear.

Appendix A

Appendix

This appendix consists of twelve actograms of mice exposed to the series of stimuli described in section 4.1.1. The data consists of wheel running data [1, 7] with wheel rotations in a five minute interval represented as a black hash. The availability of food is indicated as gray shading, and the black legend across the top indicates the phase of light exposure during portions of the training regime.

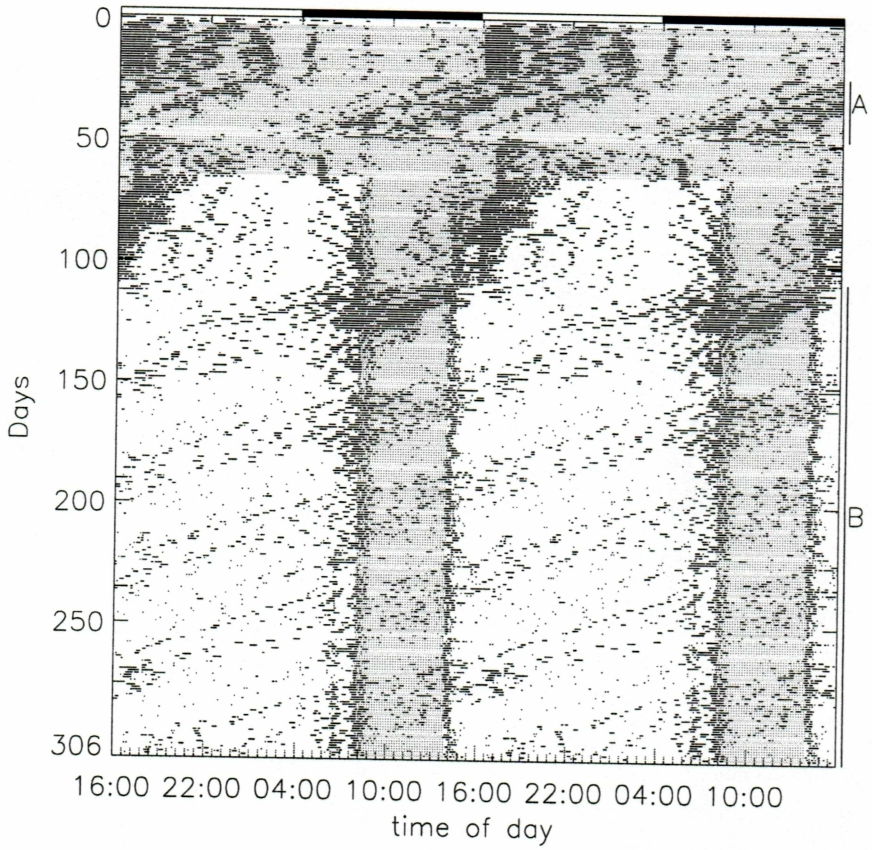

Figure A.1. Actogram of mouse 1 as shown in text.

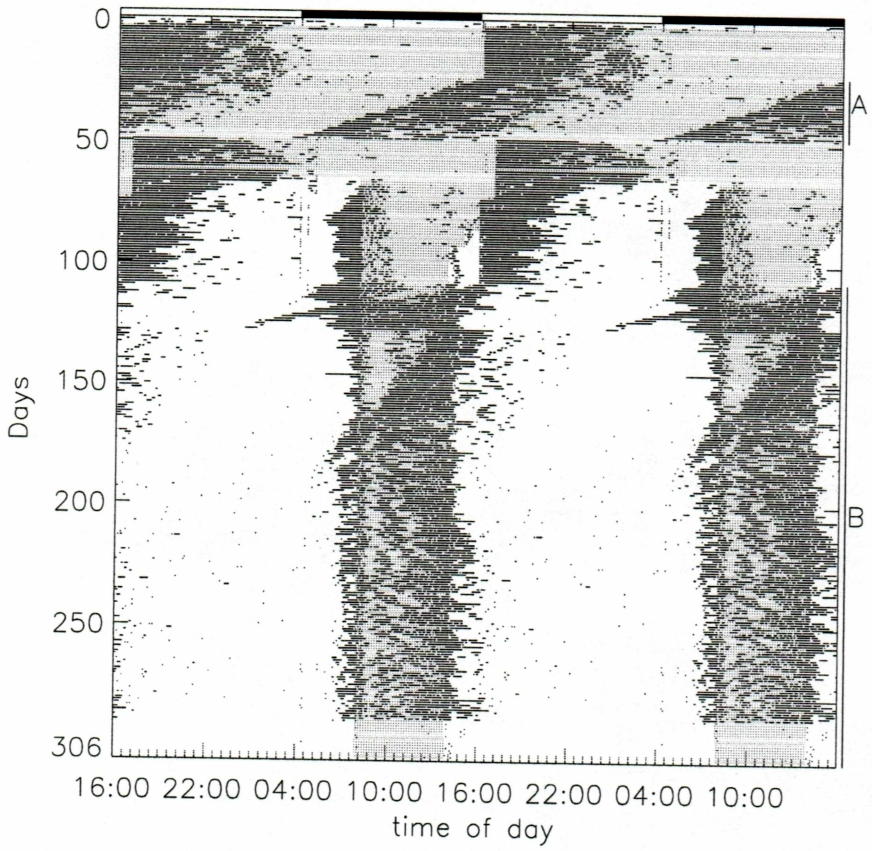

Figure A.2. Actogram of mouse 2 as shown in text.

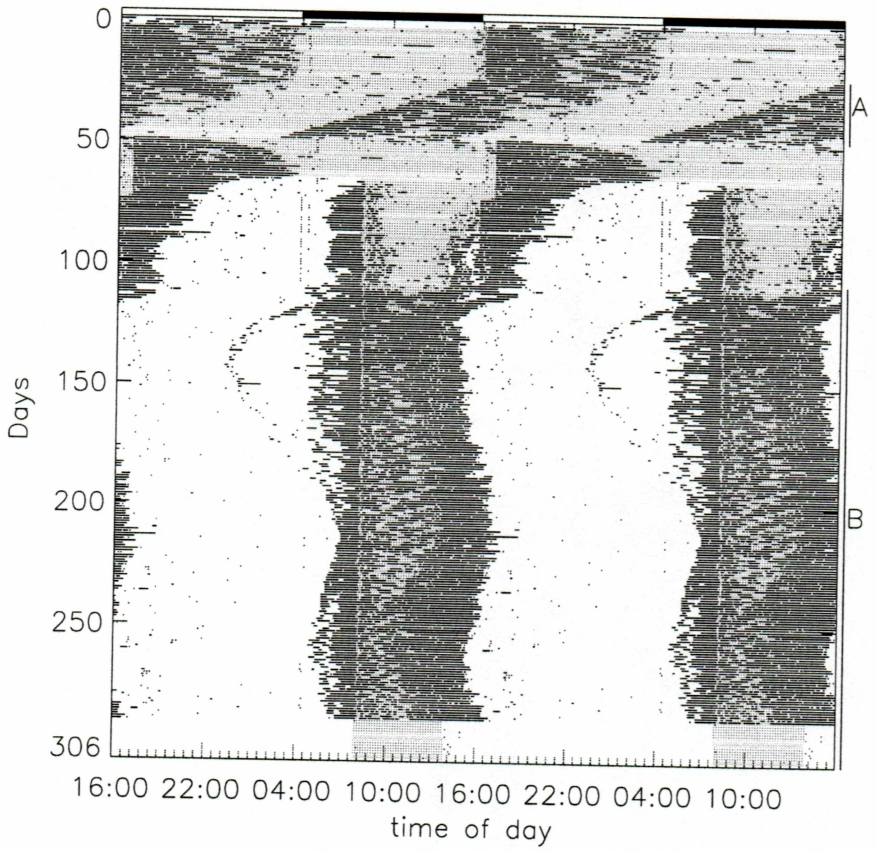

Figure A.3. Actogram of mouse 3 as shown in text.

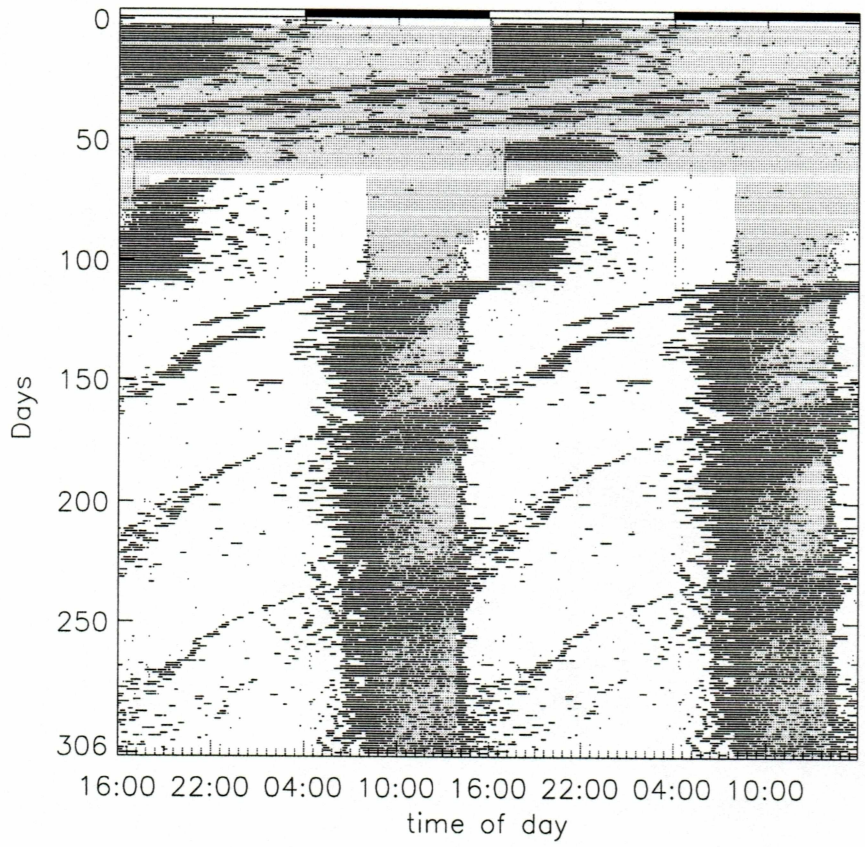

Figure A.4. Actogram of mouse 4.

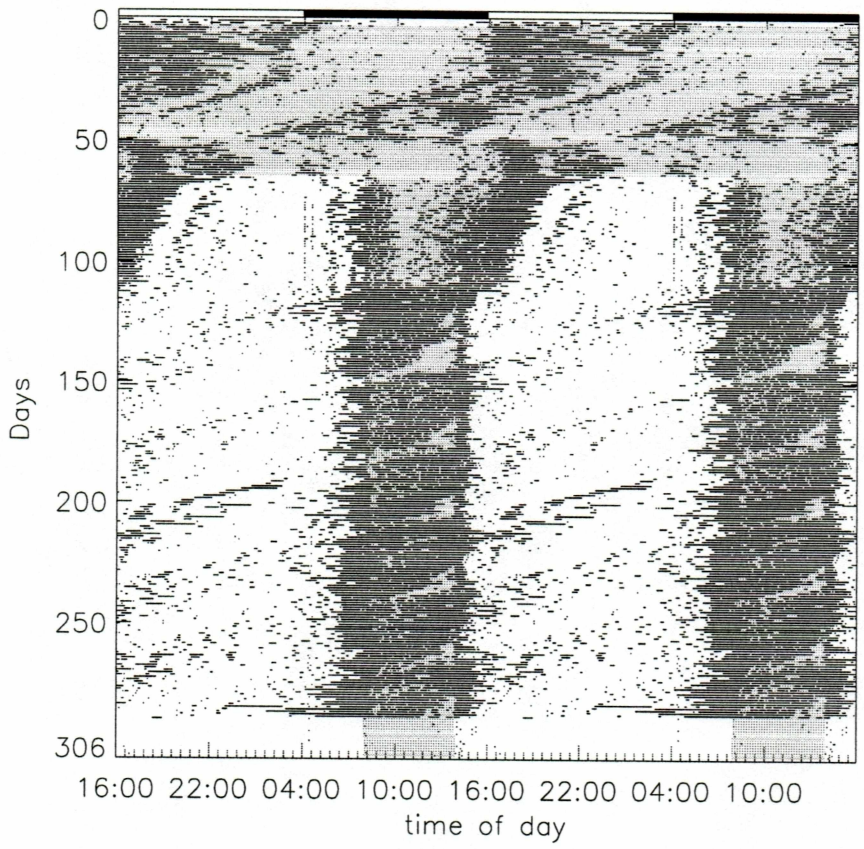

Figure A.5. Actogram of mouse 5.

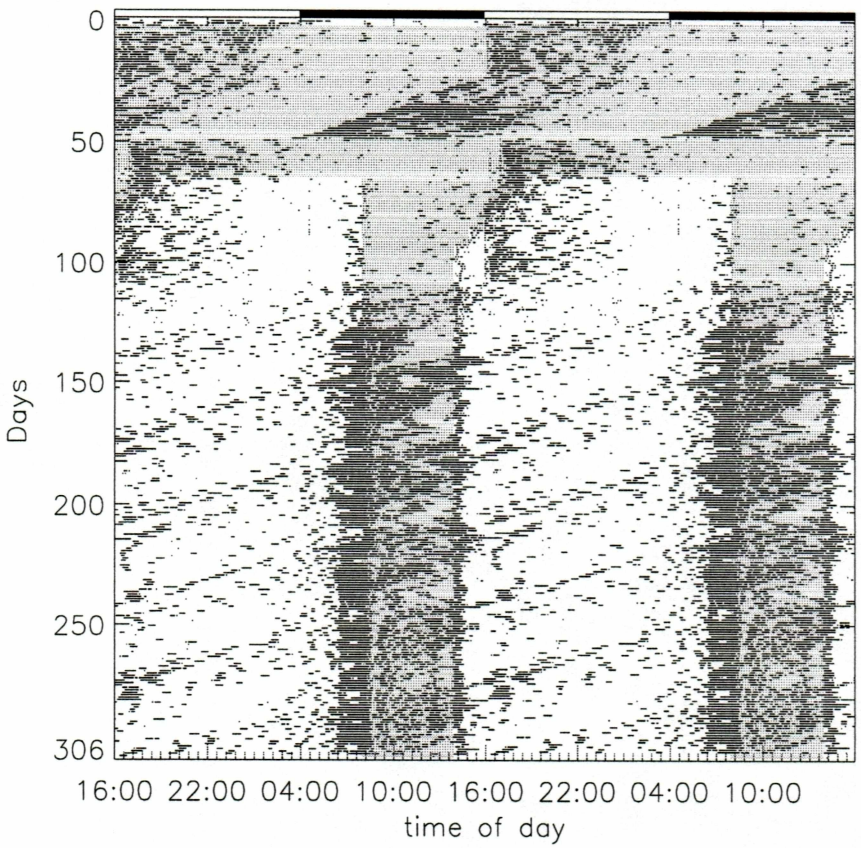

Figure A.6. Actogram of mouse 6.

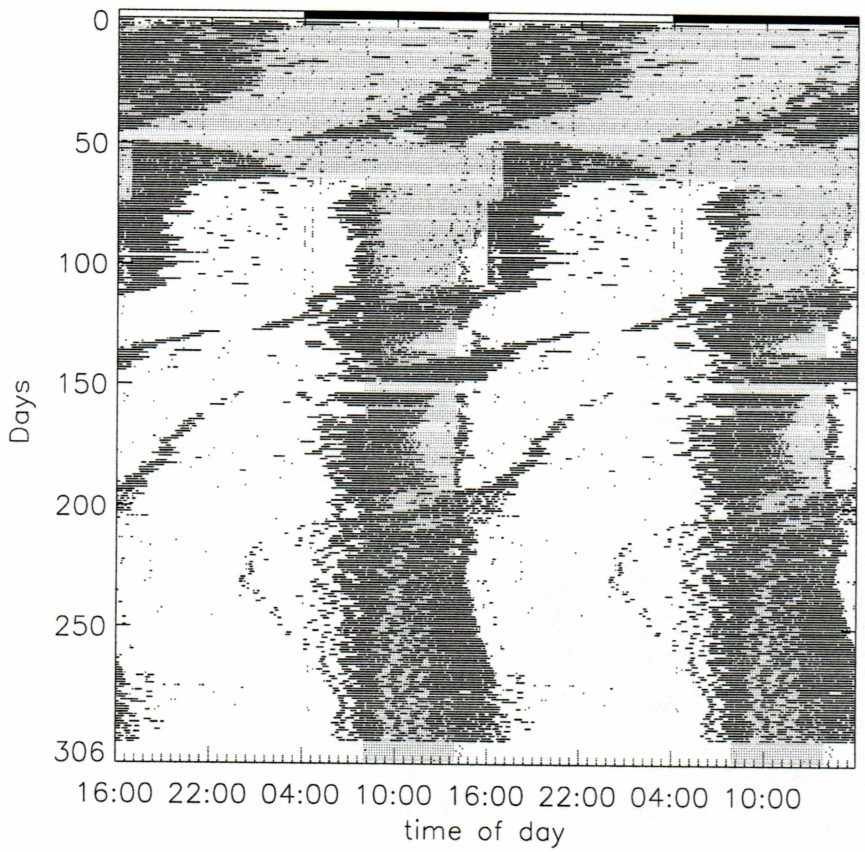

Figure A.7. Actogram of mouse 7.

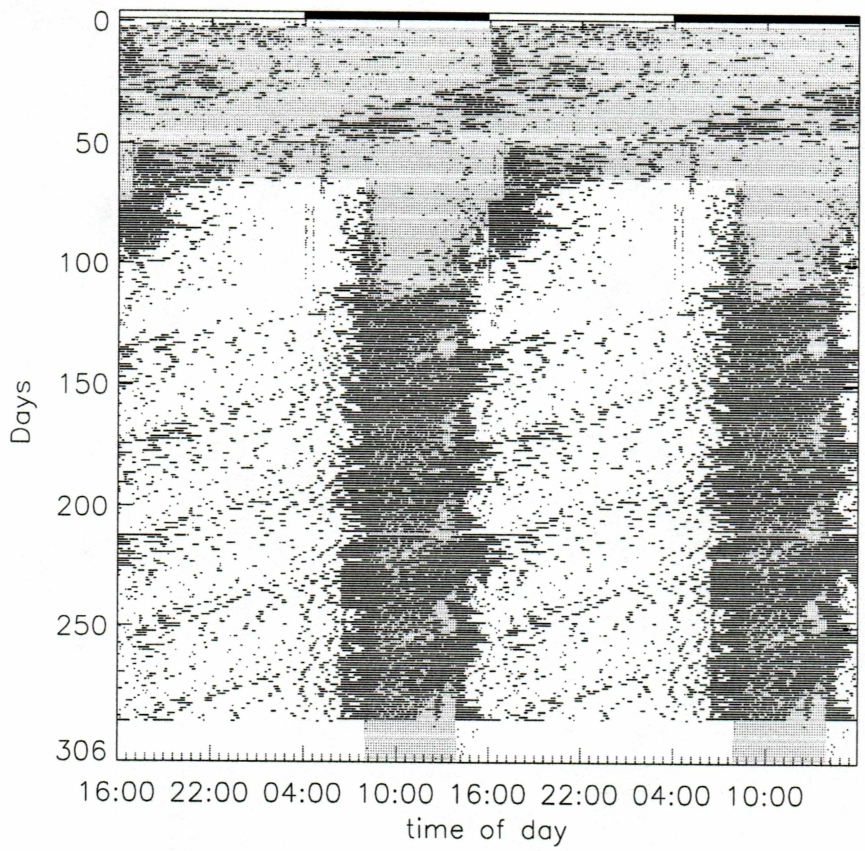

Figure A.8. Actogram of mouse 8.

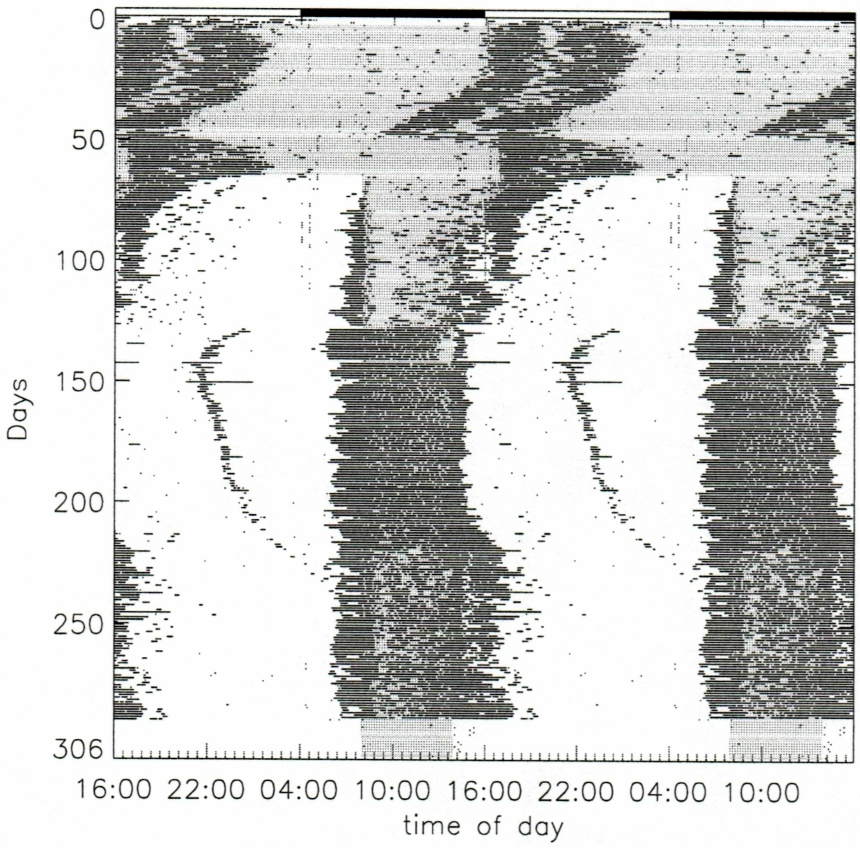

Figure A.9. Actogram of mouse 9.

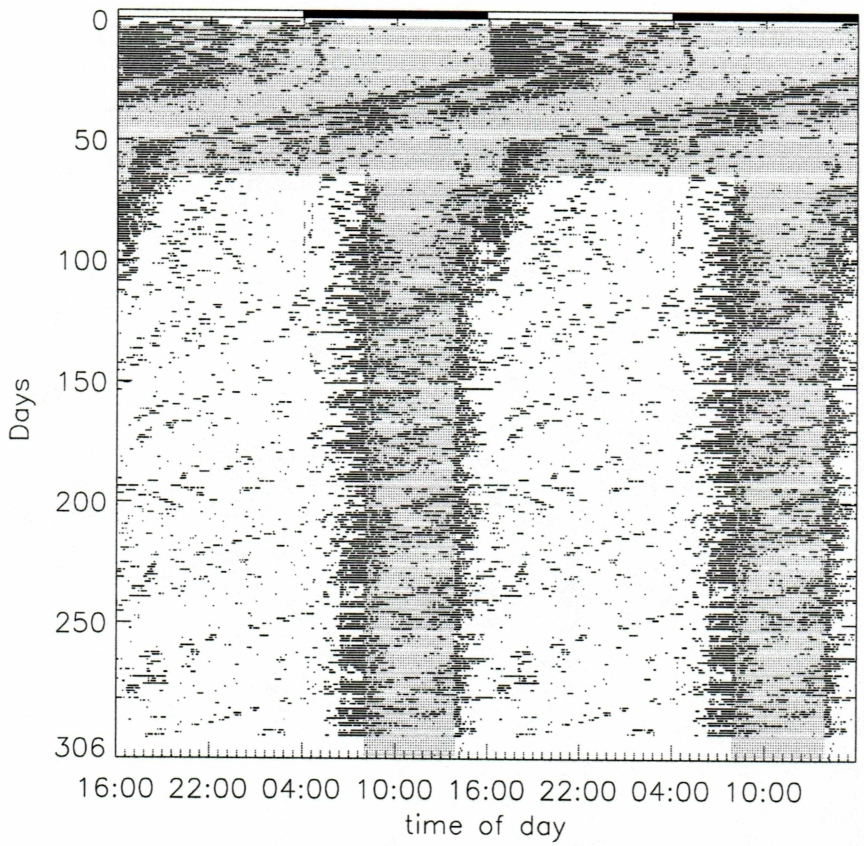

Figure A.10. Actogram of mouse 10.

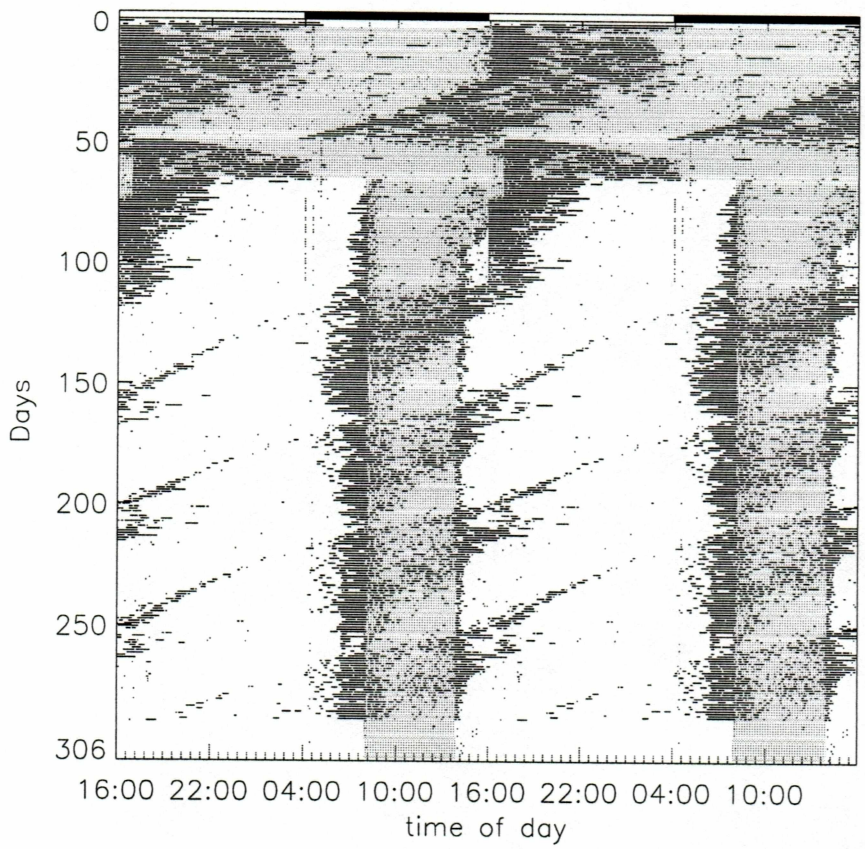

Figure A.11. Actogram of mouse 11.

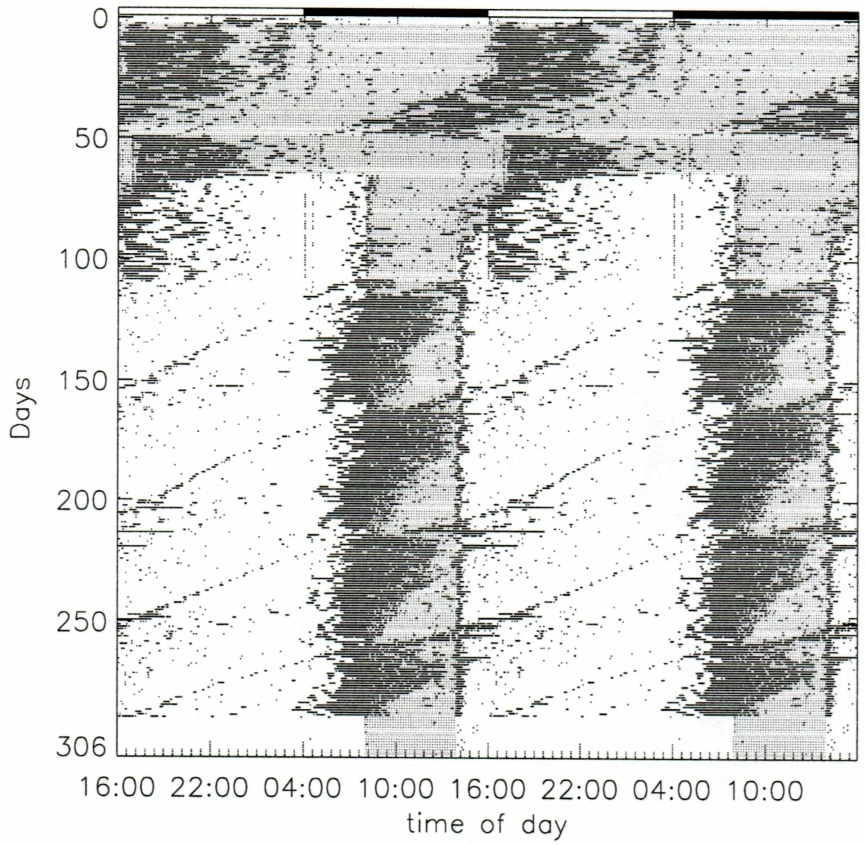

Figure A.12. Actogram of mouse 12.

References

[1] Abel Bult-Ito. Unpublished data.

[2] Dan Stoleru, Ying Peng, José Agosto, and Michael Rosbash. Coupled oscillators control morning and evening locomotor behavior of *Drosophila*. *Nature*, 431:862–868, 14 October 2004.

[3] Arthur T. Winfree. *The Geometry of Biological Time*. Springer-Verlag, 2001.

[4] http://www.medicinenet.com/script/main/art.asp?articlekey=874. Body rhythms and heart attack, 2002.

[5] Arkady Pikovsky, Michael Rosenblum, and Jürgen Kurths. *Synchronization: A universal concept in nonlinear sciences*. Cambridge University Press, 2001.

[6] Steven H. Strogatz. *Sync*. Theia, 2003.

[7] Marina R. Castillo, Kelly J. Hochstetler, Jr. Ronald J. Tavernier, Dana M. Greene, and Abel Bult-Ito. Entrainment of the master circadian clock by scheduled feeding. *Am J Physiol Regul Integr Comp Physiol*, 287:R551–R555, 2004.

[8] B. van der Pol. On "relaxation-oscillations". *The London, Edinburgh and Dublin philosophical magazine and journal of science*, 7(2):978–992, 1926.

[9] John Guckenheimer and Philip Holmes. *Nonlinear Oscillations, Dynamical Systems, and Bifurcations of Vector Fields*. Springer-Verlag, 1983.

[10] Robert C. Hilborn. *Chaos and Nonlinear Dynamics*. Oxford University Press, 1994.

[11] Steven H. Strogatz. *Nonlinear Dynamics and Chaos*. Perseus Books Publishing, 1994.

[12] Richard E. Kronauer, Charles A. Czeisler, Samuel F. Pilato, Martin C. Moore-Ede, and Elliot D. Weitzman. Mathematical model of the human circadian system with two interacting oscillators. *American Journal of Physiology*, 242:R3–R17, 1982.

[13] George B. Arfken and Hans J. Weber. *Mathematical Methods for Physicists*. Harcourt Academic Press, fifth edition, 2001.

[14] Michael G. Rosenblum, Arkady S. Pikovsky, and Jurgen Kurths. Phase synchronization of chaotic oscillators. *Phys. Rev. Lett.*, 76(11):1804–1807, 1996.

[15] R. Quian Quiroga, A. Kraskov, T. Kreuz, and P. Grassberger. Performance of different synchronization measures in real data: A case study on electroencephalographic signals. *Phys. Rev. E*, 65:041903, 2002.

[16] David J. DeShazer, Romulus Breban, Edward Ott, and Rajarshi Roy. Detecting phase synchronization in a chaotic laser array. *Phys. Rev. Lett.*, 87(4):044101, 2001.

[17] Carsten Schafer, Michael G. Rosenblum, Hans-Henning Abel, and Jurgen Kurths. Synchronization in the human cardiorespiratory system. *Phys. Rev. E*, 60(1):857–870, 1999.

[18] Romulus Breban and Edward Ott. Phase synchronization of chaotic attractors in the presence of two competing periodic signals. *Phys. Rev. E*, 65:056219, 2002.

[19] J. Y. Chen, K. W. Wong, H. Y. Zheng, and J. W. Shuai. Phase signal coupling induced n:m phase synchronization in drive-response oscillators. *Phys. Rev. E*, 63:036214, 2001.

[20] Zhigang Zheng, Gang Hu, and Bambi Hu. Enhancement of phase synchronization through asymmetric couplings. *Phys. Rev. E*, 62(5):7501–7504, 2000.

[21] Kiyoshi Kotani, Kiyoshi Takamasu, Yosef Ashkenazy, H. Eugene Stanley, and Yoshiharu Yamamoto. Model for cardiorespiratory synchronization in humans. *Phys. Rev. E*, 65:051923, 2002.

[22] A. Stefanovska, H. Haken, P.V.E. McClintock, M. Hozic, F. Bajrović, and S. Ribaric. Reversible transitions between synchronization states of the cardiorespiratory system. *Phys. Rev. Lett.*, 85(22):4831–4834, 2000.

[23] Andrew Cumming and Paul S. Linsay. Deviations from universality in the transition from quasiperiodicity to chaos. *Phys. Rev. Lett.*, 59(15):1633–1636, 1987.

[24] Alan M. Rosenwasser and Norman T. Adler. Structure and function in circadian timing systems: Evidence for multiple coupled circadian oscillators. *Neuroscience & Biobehavioral Reviews*, 10(4):431–448, 1986.

[25] Steven H. Strogatz. *The mathematical structure of the human sleep-wake cycle.* Springer-Verlag, 1986.

[26] S. Machlup and T.J. Sluckin. Driven oscillations of a limit-cycle oscillator. *Journal of Theoretical Biology*, 84:119–134, 1980.

[27] Jerry B. Marion and Stephen T. Thornton. *Classical dynamics of particles and systems.* Saunders College Publishing, 1995.

[28] Charles A. Czeisler, Richard E. Kronauer, James S. Allan, Jeanne F. Duffy, Megan E. Jewett, Emery N. Brown, and Joseph M. Ronda. Bright light induction of strong (type 0) resetting of the human circadian pacemaker. *Science*, 244:1328–1333, 16 June 1989.

[29] Dale M. Edgar, William C. Dement, and Charles A. Fuller. Effect of SCN lesions on sleep in squirrel monkeys: Evidence for opponent processes in sleep-wake regulation. *The Journal of Neuroscience*, 13(3):1065–1079, 1993.

[30] William R. Holloway Jr., Hing W. Tsui, Lee J. Grota, and Gregory M. Brown. Melatonin and corticosterone regulation: Feeding time or the light:dark cycle? *Life Sciences*, 25:1837–1842, 1979.

[31] Ralph E. Mistlberger. Nonphotic entrainment of circadian activity rhythms in suprachiasmatic nuclei-ablated hamsters. *Behavioral Neuroscience*, 106(1):192–202, 1992.

[32] Robert Y. Moore. A clock for the ages. *Science*, 284:2102–2103, 1999.

[33] K. Honma and S. Honma. Non-SCN rhythm in the circadian domain. In Yvan Touitou, editor, *Biological Clocks, Mechanisms and Applications*, pages 33–40. Elsevier Science B.V., 1998.

[34] Kelly J. Hochstetler, Jr. Theodore Garland, John G. Swallow, Patrick A. Carter, and Abel Bult-Ito. Number of arginine-vasopressin neurons in the suprachiasmatic nuclei is not related to level or circadian characteristics of wheel-running activity in house mice. *Behavior Genetics*, 34(1):131–136, 2004.

[35] Megan E. Jewett, Richard E. Kronauer, and Charles A. Czeisler. Phase-amplitude resetting of the human circadian pacemaker via bright light: a further analysis. *Journal of Biological Rhythms*, 9(3-4):295–314, 1994.

[36] Francesca Damiola, Nguyet Le Minh, Nicolas Preitner, Benoit Kornmann, Fabienne Fleury-Olela, and Ueli Schibler. Restricted feeding uncouples circadian oscillators in peripheral tissues from the central pacemaker in the suprachiasmatic nucleus. *Genes & Development*, 14:2950–2961, 2000.

[37] J.F. Ruis, L.M. Talamini, J.P. Buys, and W.J. Rietveld. Effects of time of feeding on recovery of food-entrained rhythms during subsequent fasting in SCN-lesioned rats. *Physiology & Behavior*, 46:857–866, 1989.

[38] Domien G. M. Beersma and Serge Daan. Strong or weak phase resetting by light pulses in humans? *Journal of Biological Rhythms*, 8(4):340–347, 1993.

[39] Charles A. Czeisler, James S. Allan, Steven H. Strogatz, Joseph M. Ronda, Ramiro Sanchez, C. David Rios, Walter O. Freitag, Gary S. Richardson, and Richard E. Kronauer. Bright light resets the human circadian pacemaker independent of the timing of the sleep-wake cycle. *Science*, 233:667–671, 8 Aug 1986.

[40] Charles A. Czeisler, Jeanne F. Duffy, Theresa L. Shanahan, Emery N. Brown, Jude F. Mitchell, David W. Rimmer, Joseph M. Ronda, Edward J. Silva, James S. Allan, Jonathan S. Emens, Derk-Jan Dijk, and Richard E. Kronauer. Stability, precision, and near-24-hour period of the human circadian pacemaker. *Science*, 284:2177–2181, 1999.

[41] Emery N. Brown, Yong Choe, Harry Luithardt, and Charles A. Czeisler. A statistical model of the human core-temperature circadian rhythm. *American Journal of Physiology*, 279:E669–E683, 2000.

[42] Mitsuyuki Nakao, Keisuke Yamamoto, Ken-Ichi Honma, Satoko Hashimoto, Sato Honma, Norihiro Katayama, and Mitsuaki Yamamoto. A phase dynamics model of human circadian rhythms. *Journal of Biological Rhythms*, 17(5):476–489, 2002.

[43] T. Pavlidis. Populations of interacting oscillators and circadian rhythms. *Journal of Theoretical Biology*, 22:418–436, 1969.

[44] Daniel B. Forger, Megan E. Jewett, and Richard E. Kronauer. A simpler model of the human circadian pacemaker. *Journal of Biological Rhythms*, 14(6):532–537, 1999.

[45] Peter Achermann and Alexander A. Borbely. Mathematical models of sleep regulation. *Frontiers in Bioscience*, 8:s683–693, 2003.

[46] Gail A. Carpenter and Stephen Grossberg. A neural theory of circadian rhythms: Split rhythms, after-effects and motivational interactions. *Journal of Theoretical Biology*, 113:163–223, 1985.

[47] Albert Goldbeter. A model for circadian oscillations in the *Drosophila* period protein (PER). *Proc. R. Soc. Lond. B*, 261:319–324, 1995.

[48] Albert Goldbeter. Computational approaches to cellular rhythms. *Nature*, 420:238–245, 14 Nov 2002.

[49] Friedemann Kaiser. External signals and internal oscillation dynamics: Frequency coding, signal amplification and interaction mechanisms. In Yvan Touitou, editor, *Biological Clocks, Mechanisms and Applications*, pages 53–62. Elsevier Science B.V., 1998.

[50] Chen Liu, David R. Weaver, Steven H. Strogatz, and Steven M. Reppert. Cellular construction of a circadian clock: Period determination in the suprachiasmatic nuclei. *Cell*, 91:855–860, December 1997.

[51] Steven H. Strogatz. From Kuramoto to Crawford: exploring the onset of synchronization in populations of coupled oscillators. *Physica D*, 143:1–20, 2000.

[52] Zhigang Zheng, Bambi Hu, and Gang Hu. Collective phase slips and phase synchronizations in coupled oscillator systems. *Phys. Rev. E*, 62(1):402–408, 2000.

[53] Richard E. Kronauer, Megan E. Jewett, and Charles A. Czeisler. Commentary: The human circadian response to light–strong and weak resetting. *Journal of Biological Rhythms*, 8(4):351–360, 1993.

[54] Patricia L. Lakin-Thomas. Commentary: Strong or weak phase resetting by light pulses in humans. *Journal of Biological Rhythms*, 8(4):348–350, 1993.

[55] J. E. Flaherty and F. C. Hoppensteadt. Frequency entrainment of a forced van der Pol oscillator. *Studies in Applied Mathematics*, 58:5–15, 1978.

[56] Andrey B. Belogortsev and Susan R. McKay. The secondary averaging approach to the weakly nonlinear van der Pol oscillator driven by a quasiperiodic force. *Physics Letters A*, 217:15–20, 1996.

[57] Munehisa Sekikawa, Naohiko Inaba, and Takashi Tsubouchi. Chaos via duck solution breakdown in a piecewise linear van der Pol oscillator driven by an extremely small periodic perturbation. *Physica D*, 194:227–249, 2004.

[58] R. Wever. Virtual synchronization towards the limits of the range of entrainment. *Journal of Theoretical Biology*, 36:119–132, 1972.

[59] Theodosios Pavlidis. *Biological Oscillators: Their Mathematical Analysis.* Academic Press, 1973.

[60] Daniel B. Forger and Richard E. Kronauer. Reconciling mathematical models of biological clocks by averaging on approximate manifolds. *SIAM J. of Appl. Math.*, 62(4):1281–1296, 2002.

[61] Marina R. Castillo and Abel Bult-Ito. Personnal communications.

[62] William H. Press, Sual A. Teukolsky, William T. Vetterling, and Brian P. Flannery. *Numerical Recipies in Fortran: The Art of Scientific Computing.* Cambridge University Press, second edition, 1992.

[63] Martin R. Ralph, Russell G. Foster, Fred C. Davis, and Michael Menaker. Transplanted suprachiasmatic nucleus determines circadian period. *Science*, 247:975–978, 23 February 1990.

[64] Ralph E. Mistlberger. Finding food in a periodic world: The role of circadian clocks, Presentation at the University of Alaska Fairbanks on 5 December, 2003.

[65] David K. Welsh, Diomedes E. Logothetis, Markus Meister, and Steven M. Reppert. Individual neurons dissociated from rat suprachiasmatic nucleus express independently phased circadian firing rhythms. *Neuron*, 14:697–706, 1995.

[66] Erik D. Herzog, Sara J. Aton, Rika Numano, Yoshiyuki Sakaki, and Hajime Tei. Temporal precision in the mammalian circadian system: A reliable clock from less reliable neurons. *Journal of Biological Rhythms*, 19(1):35–46, 2004.

[67] Horacio O. de la Iglesia, Jennifer Meyer, Alan Carpino Jr., and William J. Schwartz. Antiphase oscillation of the left and right suprachiasmatic nuclei. *Science*, 290(5492):799–801, 2000.

[68] Paul C. Matthews and Steven H. Strogatz. Phase diagram for the collective behavior of limit-cycle oscillators. *Phys. Rev. Lett.*, 65(14):1701–1704, 1990.

[69] R. Mettin, U. Parlitz, and W. Lauterborn. Bifurcation structure of the driven van der Pol oscillator. *International Journal of Bifurcation and Chaos*, 3(6):1529–1555, 1993.